Terrestrial Evaporation and Global Climate: Lessons from Northland, a Planet with a Hemispheric Continent

MARYSA M. LAGUË,[a,b] MARIANNE PIETSCHNIG,[c] SARAH RAGEN,[d] TIMOTHY A. SMITH,[e] AND DAVID S. BATTISTI[f]

[a] *Department of Earth and Planetary Science, University of California Berkeley, Berkeley, California*
[b] *University of Saskatchewan Coldwater Lab, Canmore, Alberta, Canada*
[c] *Department of Mathematics, University of Exeter, Exeter, United Kingdom*
[d] *School of Oceanography, University of Washington, Seattle, Washington*
[e] *Oden Institute for Computational Engineering and Sciences, The University of Texas at Austin, Austin, Texas*
[f] *Department of Atmospheric Sciences, University of Washington, Seattle, Washington*

(Manuscript received 11 June 2020, in final form 10 December 2020)

ABSTRACT: Motivated by the hemispheric asymmetry of land distribution on Earth, we explore the climate of Northland, a highly idealized planet with a Northern Hemisphere continent and a Southern Hemisphere ocean. The climate of Northland can be separated into four distinct regions: the Southern Hemisphere ocean, the seasonally wet tropics, the midlatitude desert, and the Great Northern Swamp. We evaluate how modifying land surface properties on Northland drives changes in temperatures, precipitation patterns, the global energy budget, and atmospheric dynamics. We observe a surprising response to changes in land surface evaporation, where suppressing terrestrial evaporation in Northland cools both land and ocean. In previous studies, suppressing terrestrial evaporation has been found to lead to local warming by reducing latent cooling of the land surface. However, reduced evaporation can also decrease atmospheric water vapor, reducing the strength of the greenhouse effect and leading to large-scale cooling. We use a set of idealized climate model simulations to show that suppressing terrestrial evaporation over Northern Hemisphere continents of varying size can lead to either warming or cooling of the land surface, depending on which of these competing effects dominates. We find that a combination of total land area and contiguous continent size controls the balance between local warming from reduced latent heat flux and large-scale cooling from reduced atmospheric water vapor. Finally, we demonstrate how terrestrial heat capacity, albedo, and evaporation all modulate the location of the ITCZ both over the continent and over the ocean.

KEYWORDS: Energy transport; Atmosphere-land interaction; Climatology; Evaporation; Water vapor; Climate models; General circulation models

1. Introduction

The physical properties of the land surface and the ocean differ in several fundamental ways. For instance, land has a much lower heat capacity than ocean (Cess and Goldenberg 1981; North et al. 1983; Bonan 2008), land has a higher albedo than ocean (Budyko 1961, 1969; Payne 1972; Bonan 2008), the ocean has the ability to move heat laterally (Loft 1918; Richardson 1980; Trenberth and Caron 2001; Ferrari and Ferreira 2011; Forget and Ferreira 2019), and there are large climatic impacts of terrestrial orography (Queney 1948; Eliassen and Palm 1960; Manabe and Terpstra 1974; Held et al. 1985; McFarlane 1987). Moreover, land stores and evaporates less water than ocean, and soil and vegetation properties provide resistance to evaporation over land (Manabe 1969; Bonan 2008, and references therein). The contrasts between physical properties of land and ocean are important controls on atmospheric dynamics, profoundly impacting the climate. The hemispheric asymmetry in land–sea distribution has implications for global climate, including the higher sensitivity of the Northern Hemisphere to increases in anthropogenic greenhouse gases (Manabe et al. 1991; Stouffer et al. 1989). In this study, we focus on how the limited capacity of the land to hold water, its small heat capacity, and its higher albedo alter the climate system.

The albedo of different land types is much higher than that of ice-free ocean. Land albedo ranges from 0.05–0.25 (vegetated) to 0.5–0.9 (glaciers and snow) (Wiscombe and Warren 1980; Oke 1987; Bonan 2008). In contrast, the surface albedo of the ice-free ocean is generally less than 0.1 (Jin et al. 2004). The difference in top-of-atmosphere (TOA) albedo between land and ocean is less drastic, with TOA albedo ranging from 0.25 to 0.6 over snow-free land, and from 0.1 to 0.5 over ice-free ocean for Earth in the present climate. These higher values result from atmospheric controls on the TOA albedo, via the effects of cloud cover, aerosols, and attenuation (Donohoe and Battisti 2011).

Additionally, land has a much smaller heat capacity than the ocean, and a limited ability to move energy laterally. Oceans can absorb large amounts of energy (Kuhlbrodt and Gregory 2012; Cheng et al. 2017) and transport energy via ocean currents; there are areas of the ocean that can continually take up energy, while other regions act as a source of energy to the atmosphere (e.g., Marshall and Zanna 2014; Forget and Ferreira 2019). In contrast, energy absorbed at one location on land generally must be released back to the atmosphere at that

Supplemental information related to this paper is available at the Journals Online website: https://doi.org/10.1175/JCLI-D-20-0452.s1.

Corresponding author: Marysa M. Laguë, mlague@uw.edu

DOI: 10.1175/JCLI-D-20-0452.1

same location in the form of upward longwave radiation, sensible heat, or latent heat (evaporation). While the land can store energy on seasonal time scales, the seasonal storage of heat by the land surface is much smaller than that of the ocean (Marshall and Plumb 2007). The annual mean heat storage of a land surface in equilibrium is near zero (Budyko 1974; Milly and Shmakin 2002).

The limited capacity of the land surface to hold water and the increased resistance to evaporation over land surfaces compared to over open water drastically alters evaporative fluxes over land. Over the ocean, evaporation is determined mainly by the meteorological conditions at the atmosphere–ocean interface (e.g., the surface temperature and atmospheric humidity). In contrast, dry land surfaces have little water available for evaporation, and thus little evaporation occurs regardless of the evaporative demand of the overlying atmosphere. Various properties of soil and vegetation further modulate the availability of water to the atmosphere, including total leaf area and roots that can provide access to water deep in the soil column (Canadell et al. 1996; Bonan 2008). Moreover, plants directly regulate the movement of water from the land to the atmosphere by opening and closing their stomata (small pores on leaves that modulate gas exchange) (Sellers et al. 1996).

These fundamental physical differences between land and ocean result in very different surface–atmosphere interactions. Changes in land surface properties can modify the global climate system (Charney 1975; Shukla and Mintz 1982; Sud et al. 1988; Davin and de Noblet-Ducoudré 2010; Laguë et al. 2019). Large hemispheric energy imbalances, such as those generated by sea ice, large-scale vegetation change, or an idealized energy source, can drive large-scale changes in the location of the zonal mean intertropical convergence zone (ITCZ) and the Hadley circulation (Chiang and Bitz 2005; Broccoli et al. 2006; Kang et al. 2008; Swann et al. 2012; Laguë and Swann 2016; Kang 2020). In response to a hemispheric energy imbalance, the rising branch of the Hadley circulation moves toward the energy-rich hemisphere, thereby moving energy toward the energy-poor hemisphere and shifting the ITCZ toward the energy-rich hemisphere (Donohoe et al. 2013), provided there are no large changes in gross moist stability [see Geen et al. (2020) and references therein]. The distribution of land impacts climate in myriad ways, including by directing storm tracks, shaping ocean circulation, generating planetary waves, and impacting orographic forcing and diabatic heating of the atmosphere (Eliassen and Palm 1960; Hartmann 1994; Donohoe et al. 2020).

At present, 68% of land on Earth is in the Northern Hemisphere (NH) and 32% is in the Southern Hemisphere (SH). The hemispheric asymmetry in this distribution of land has long been thought to drive asymmetries in surface temperature (Croll 1870; Stouffer et al. 1989; Manabe et al. 1991), precipitation, and ocean heat transport (Nilsson et al. 2013). In this study we investigate the climatic implications of the asymmetry in the distribution of land between the SH and the NH. We use an atmospheric general circulation model to explore how fundamental differences between the land and ocean affect the climate. We model the climate of a hypothetical planet that is Earth-like in size and orbital configuration, but has an idealized continent covering the entire NH, and an ocean covering the entire SH. We explore the mean state of this planet, which we call Northland, and probe how modifying the albedo of the land surface and its capacity to hold water alter the planet's climate. We also explore the climate of several alternative continental configurations, and consider a land-covered planet.

Idealized models are a useful tool in climate science as they help to narrow the gap between simulating the climate system and understanding its mechanisms, as highlighted in Sellers (1969), Held (2005), Jeevanjee et al. (2017), and Maher et al. (2019). Idealized models can be traced back to "Galilean" idealizations, in which a problem is simplified to make it easier to solve (McMullin 1985). While an idealized model sacrifices realistic representations of physical processes, this approach aides in illuminating fundamental processes of the climate system (Levins 1966)—in this case, differences between land and ocean surface interactions with the atmosphere.

2. Methods

a. Model

We use Isca (Vallis et al. 2018), a framework for designing idealized atmospheric general circulation models (GCMs), to explore the climate of an Earth-like planet with an idealized continental configuration. The atmosphere is coupled to a 20-m slab ocean without any ocean heat transport in our simulations. Land grid cells differ from ocean grid cells by having a higher albedo, smaller heat capacity, a finite reservoir of water, and a parameterized representation of soil moisture that leads to a reduction in evaporation when the soil is less than saturated. The land parameterization used in this study is similar to that of Manabe (1969), where land hydrology is represented using a bucket model. In this model configuration, there is no snow or sea ice, and thus no representation of surface albedo feedbacks that would amplify cooling when surface temperatures drop below freezing; soil moisture does not impact land surface albedo.

The atmosphere uses moist dynamics, but does not represent clouds. While cloud responses to land surface properties and their changes can play an important role in determining impacts on surface climate (Cho et al. 2018; Sikma and Vilà-Guerau de Arellano 2019; Laguë et al. 2019; Kim et al. 2020), cloud responses to climate perturbations are also a large source of uncertainty (IPCC 2013; Zelinka et al. 2017). Our idealized modeling framework avoids uncertainties associated with cloud responses to climate perturbations, at the cost of not capturing any cloud interaction effects. The surface albedo α of both water ($\alpha_{\text{ocean}} = 0.25$) and land ($\alpha_{\text{land}} = 0.325$; Table 1) is higher than it would be in a model that included clouds, to allow for a more realistic planetary albedo at the top of the atmosphere (Donohoe and Battisti 2011). Despite the absence of clouds, the model still produces precipitation [see Vallis et al. (2018) for details]. Simulations are run using a T42 horizontal resolution (roughly 2.8° latitude × 2.8° longitude) with 40 vertical levels.

TABLE 1. List of the idealized-continent Isca simulations used in this study, along with the land surface property values for each experiment.

Experiment name	Description	Land albedo	Bucket depth (m H_20)	Initial water in bucket (m H_20)
NorthlandBright	Northern Hemisphere continent with an albedo brighter than the ocean	0.325	0.15	0.1
NorthlandDark	Northern Hemisphere continent with the same albedo as the ocean	0.25	0.15	0.1
NorthlandEmpty	Like NorthlandBright, but initialized with no water on the land surface	0.325	0.15	0
NorthlandDry	Like NorthlandBright, but with a very small capacity for the land to hold water	0.325	0.000 01	0
Lakeworld	All-land planet with bucket hydrology modified to allow lakes to form	0.325	0.15	0.1
NorthWestLand	Single 180°-longitude-wide continent from 0° from 90°N, covering 25% of the planet's surface; land surface properties same as NorthlandBright	0.325	0.15	0.1
NorthWestLandDry	Same as NorthWestLand, but with the same land surface properties as as NorthlandDry	0.325	0.000 01	0
ThreeQuarterLand	Single 270°-longitude-wide continent from 0° to 90°N, covering 75% of the NH (3/8 of the total planetary surface); land surface properties same as NorthlandBright	0.325	0.15	0.1
ThreeQuarterLandDry	Same as ThreeQuarterLand, but with the same land surface properties as NorthlandDry	0.325	0.000 01	0
TwoPatchLand	Two equally spaced 90°-longitude-wide continents from 0° to 90°N, covering a combined total 25% of the planet's surface; land surface properties same as NorthlandBright	0.325	0.15	0.1
TwoPatchLandDry	Same as TwoPatchLand, but with the land surface properties the same as NorthlandDry	0.325	0.000 01	0
ThreePatchLand	Three equally spaced 90°-longitude-wide continents from 0° to 90°N, covering a combined total 75% of the NH; land surface properties same as NorthlandBright	0.325	0.15	0.1
ThreePatchLandDry	Same as ThreePatchLand, but with the land surface properties the same as NorthlandDry	0.325	0.000 01	0
Aqua	Aquaplanet simulation with 20-m mixed layer (no land)	—	—	—

b. *Experiments*

We run a total of 14 simulations, with six continental configurations and various land surface properties modified between simulations (Table 1). In all simulations, there is a seasonal cycle in insolation (obliquity = 23.439°, eccentricity = 0) with a 360-day year; atmospheric CO_2 concentrations are fixed at 300 ppm. We refer to the six continental configurations as Northland, ThreeQuarterLand, North WestLand, ThreePatchLand, TwoPatchLand, and Lakeworld (Fig. 1). Lakeworld is entirely land with no ocean, while TwoPatchLand, ThreePatchLand, NorthWestLand, ThreeQuarterLand, and Northland have an SH ocean and land covering between half and all of the NH (see Table 1 and Fig. 1 for details).

For the Northland continental configuration, we consider four simulations with varied land surface properties; we refer to these simulations as ''NorthlandXX'' (where ''XX'' indicates a specific simulation). Our ''control'' simulation (to which we generally compare our other experiments) is called NorthlandBright. In NorthlandBright, the NH continent has an albedo that is 1.3 times that of the ocean (α_{land} = 0.325, α_{ocean} = 0.25). The heat capacity of the land is 1/10 that of the

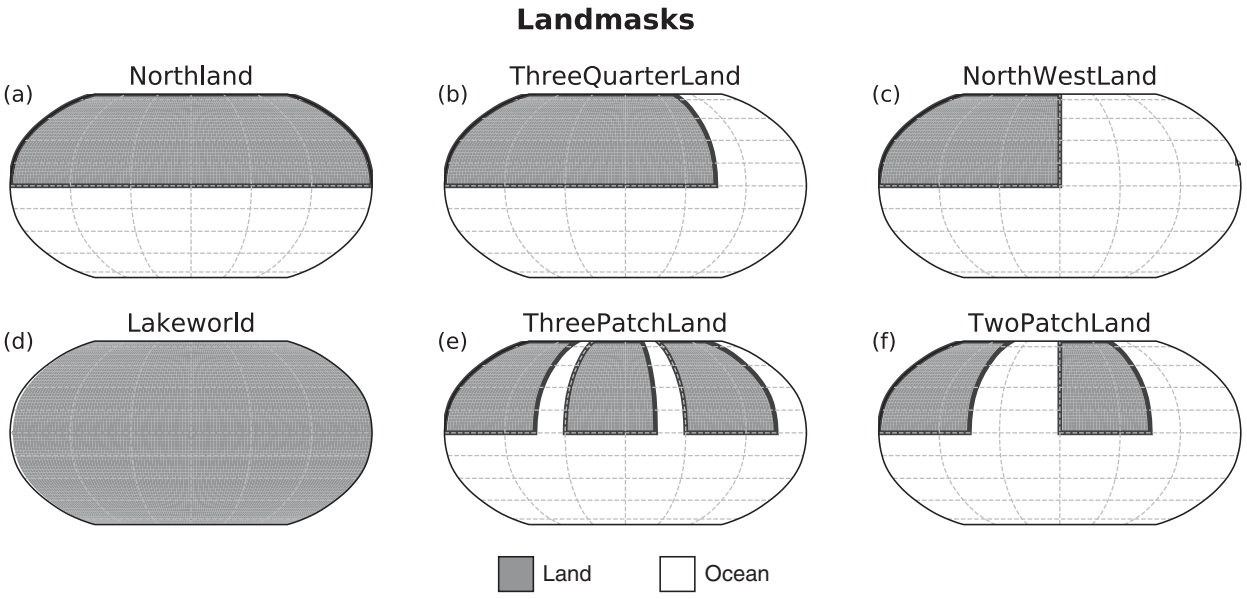

FIG. 1. Maps of the continental distributions used in this study. Gray areas indicate land, while white areas indicate ocean.

ocean in our simulations (i.e., equivalent to a 2-m mixed layer ocean). This is larger than the heat capacity of land on Earth, but Isca simulations with realistic continents have been shown to compare well with reanalyses when these heat capacities are used (Thomson and Vallis 2019; Geen et al. 2018). The roughness length is 0.2 mm and is uniform over land and ocean in our simulations. Hydrology is represented by the "bucket model" (Manabe 1969; Vallis et al. 2018), where the capacity of the land to hold water ("bucket capacity") is set to 150 mm in our simulations, and water on land is initialized everywhere at 100 mm. The bucket receives water when precipitation exceeds evaporation and loses water when the opposite occurs. When the bucket is more than 3/4 full, the resistance to evaporating water from the land surface is the same as over open water. When the bucket is less than 3/4 full, evaporative resistance scales inversely with the amount of water in the bucket.

We run three additional Northland experiments to demonstrate various aspects of the land surface's impact on the climate system. In each of these simulations, a single property of the land surface is modified compared to NorthlandBright. In the NorthlandDark experiment, the albedo of the land is reduced so that it is the same as the ocean ($\alpha_{land} = \alpha_{ocean} = 0.25$). In the NorthlandEmpty experiment, the land surface is initialized with no water on the land surface; thus, all water that ends up on land must have originated from the SH ocean. NorthlandEmpty differs from NorthlandBright only in the initial conditions. In the NorthlandDry experiment, the capacity of the land to hold water is greatly reduced, to near-zero (0.01 mm). This effectively shuts off evaporation from the land surface.

For each of the NorthWestLand, ThreeQuarterLand, TwoPatchLand, and ThreePatchLand continental configurations, we run two simulations. In NorthWestLand, ThreeQuarterLand, TwoPatchLand, and ThreePatchLand, the land surface has the same properties as NorthlandBright. In NorthWestLandDry, ThreeQuarterLandDry, TwoPatchLandDry, and ThreePatchLandDry, the land surface has the same properties as NorthlandDry (i.e., terrestrial evaporation is suppressed).

We run one simulation where the entire planet is covered with land. We refer to this simulation as Lakeworld. Lakeworld has the same albedo as NorthlandBright $\alpha_{land} = 0.325$, but the bucket hydrology is modified to allow the land to form lakes over grid cells that receive precipitation when the bucket is already full. When the soil moisture is less than 150 mm, the same rules governing terrestrial evaporation in NorthlandBright apply. However, the soil is allowed to accumulate an infinite amount of water. When the soil moisture exceeds 150 mm, the same rules of evaporation for fully saturated soils (which in these simulations are the same as the rules for open water) apply. The lakes do not impact land albedo or heat capacity. Last, we run an aquaplanet simulation (called Aqua) with no land, where the whole planet is covered with a 20-m-deep mixed layer slab ocean, with an albedo of $\alpha_{ocean} = 0.25$.

Most simulations were run for 20 years, though some Northland simulations were run for 50 years to check model drift, and Lakeworld was run for 80 years due to the unique water cycle of the all-land planet. The first four years of each simulation are discarded to allow for model spinup, after which time there is a global-mean drift in surface temperatures of less than 0.01 K yr^{-1} in the Northland and Aqua simulations (see Fig. S1 in the online supplemental material). Unless otherwise stated, the results presented here are taken from years 5–20 of the simulations (5–80 for Lakeworld). The Lakeworld simulation does not reach equilibrium in 80 years (Fig. S1), but this simulation is used to demonstrate the transient migration of water, rather than explored for its equilibrium climate.

When statistical significance is shown for a difference between two experiments, Student's t test is used, with $p < 0.05$ indicating 95% confidence that the simulations differ significantly. When error bars are used, they represent ±1 standard deviation. Analysis was conducted using the Python programming language, heavily leveraging the NumPy (Harris et al. 2020) and xarray (Hoyer and Hamman 2017) packages.

3. Results

Here our goal is to explore the factors that control the surface energy and hydrologic budgets of the idealized Northland planet. We begin with an overview of the climatology in the NorthlandBright experiment (section 3a), which we view as a control simulation. We then investigate how changes in land albedo (section 3b) and terrestrial evaporation (section 3c) impact the temperature and water cycle of the planet. Next, we explore the effect of suppressing terrestrial evaporation with alternate configurations that include some ocean in the NH (section 3d). Finally, we explore the role of moisture transport (section 3e) and show that the mere presence of a continent causes the ITCZ to extend farther poleward than in a pure aquaplanet setting (section 3f).

a. *NorthlandBright (control simulation) climatology*

NorthlandBright can be divided into four distinct climatic zones: the SH ocean, the seasonally wet tropical land belt, the NH midlatitude desert, and the NH moist high-latitude region. The mean climate of the NorthlandBright simulation reflects a world where the area-weighted annual mean surface temperature over the continent is slightly cooler (277 K) than over the ocean (280 K) (see Table S1 in the online supplemental material); this is unlike present-day Earth, where—in the extratropics—land regions are generally slightly warmer than ocean regions (Wallace et al. 1995; Sutton et al. 2007). The continent has a much larger seasonal cycle of temperature than the ocean, reflecting its smaller heat capacity (Fig. 2; see also Table S1). The hottest part of the continent, with temperatures reaching 304 K, occurs around 30°N during NH summer, while temperatures near the North Pole plunge to 220 K during NH winter (Fig. 2a). Temperatures and seasonality over the SH ocean are much more moderate, with a hemispherically averaged temperature difference of only 4 K between summer and winter, compared to 34 K in the NH (Table S1).

The globally averaged annual mean rainfall in the NorthlandBright simulation is approximately 2 mm day^{-1}. Unsurprisingly, more of this rain falls over the ocean (2.9 mm day^{-1}) than over the continent (1.5 mm day^{-1}), with a strong latitudinal dependence (Fig. 2b). The ITCZ has a strong seasonal cycle, with heavier rainfall and a peak that extends farther poleward over the ocean than over the continent (Figs. 2b and 3a). Over the continent, the ITCZ reaches its farthest poleward extent during August and September, with the peak in precipitation reaching approximately 15°N. In contrast, the peak in the ITCZ over the ocean occurs at around 20°S during March, with roughly double the rate of precipitation in the ocean ITCZ peak compared to the land ITCZ peak. The land cannot support as strong an ITCZ because much of the moisture for the ITCZ must initially be brought onto the land each season by ITCZ precipitation; in contrast, the ocean provides an unlimited supply of water in the form of local evaporation that can subsequently be precipitated in the SH ITCZ.

Terrestrial tropical precipitation is most intense from August to November. The land water evaporates quickly in the tropics due to high insolation (i.e., evaporation has a similar seasonal cycle to precipitation; Figs. 3a–c). North of 20°N, precipitation is roughly equal to evaporation in the annual mean (not shown). Despite heavy wet-season precipitation in the tropics, the ground between 0° and 20°N dries out during the dry season (February–June), because of strong seasonal evaporation (Figs. 3b,d).

In the subtropics of the land hemisphere (roughly 20°–40°N) there is a desert with dry soil year-round (Figs. 2b and 3d). Extratropical precipitation in the land hemisphere features a broad maximum in NH summer that extends from 50°N to the pole that is likely due to localized convection (Fig. 2b). In the ocean hemisphere, the extratropical maximum in precipitation is located at about 40°S, and is storm track precipitation associated with baroclinic cyclones (Fig. 2b). Precipitation in the ocean hemisphere storm track is nearly seasonally invariant.

The high-latitude soil is saturated or nearly saturated with water year-round, forming what we call the "Great Northern Swamp" (Fig. 3d), with slightly less terrestrial water storage during June–July when evaporation (fueled by increased summer insolation) exceeds precipitation (Figs. 3c,d). Interestingly, the soil moisture in the Great Northern Swamp is supplied by water transport from the tropics, and not from local moisture recycling alone. This becomes clear when the land is initialized without any water (NorthlandEmpty). In this simulation, the high-latitude soil water is indistinguishable from NorthlandBright within 4–5 years (Figs. 3d,e). The transport of water to the poles is explored further in section 3e.

b. *Climate impacts of land albedo*

As we would expect, reducing the albedo of the land surface (making the land darker) leads to surface warming. In NorthlandDark, the land albedo is the same as that of the ocean. As such, the land hemisphere absorbs more solar energy in NorthlandDark than in NorthlandBright (Fig. S2b), leading to greater temperatures year-round (Fig. 2c). The additional shortwave (SW) radiation absorbed in NorthlandDark compared to NorthlandBright is released to the atmosphere in the form of longwave (LW) radiation, sensible heat, or latent heat (Figs. S2c–f). Increased temperatures and increased water vapor (resulting in similar relative humidity over the continent between NorthlandDark and NorthlandBright; Fig. 2e) lead to more downwelling longwave radiation at the surface (Fig. S2a). That is, the warming in NorthlandDark is due to increased SW absorption as well as increased downwelling LW at the surface. NorthlandDark is warmer than NorthlandBright over both land (+7.4 K; Fig. 2c and Table S1) and ocean (+2.4 K; Fig. 2c and Table S1), due to atmospheric transport of water vapor and heat. The continent in NorthlandDark is not only warmer than NorthlandBright; it is also wetter, particularly during the

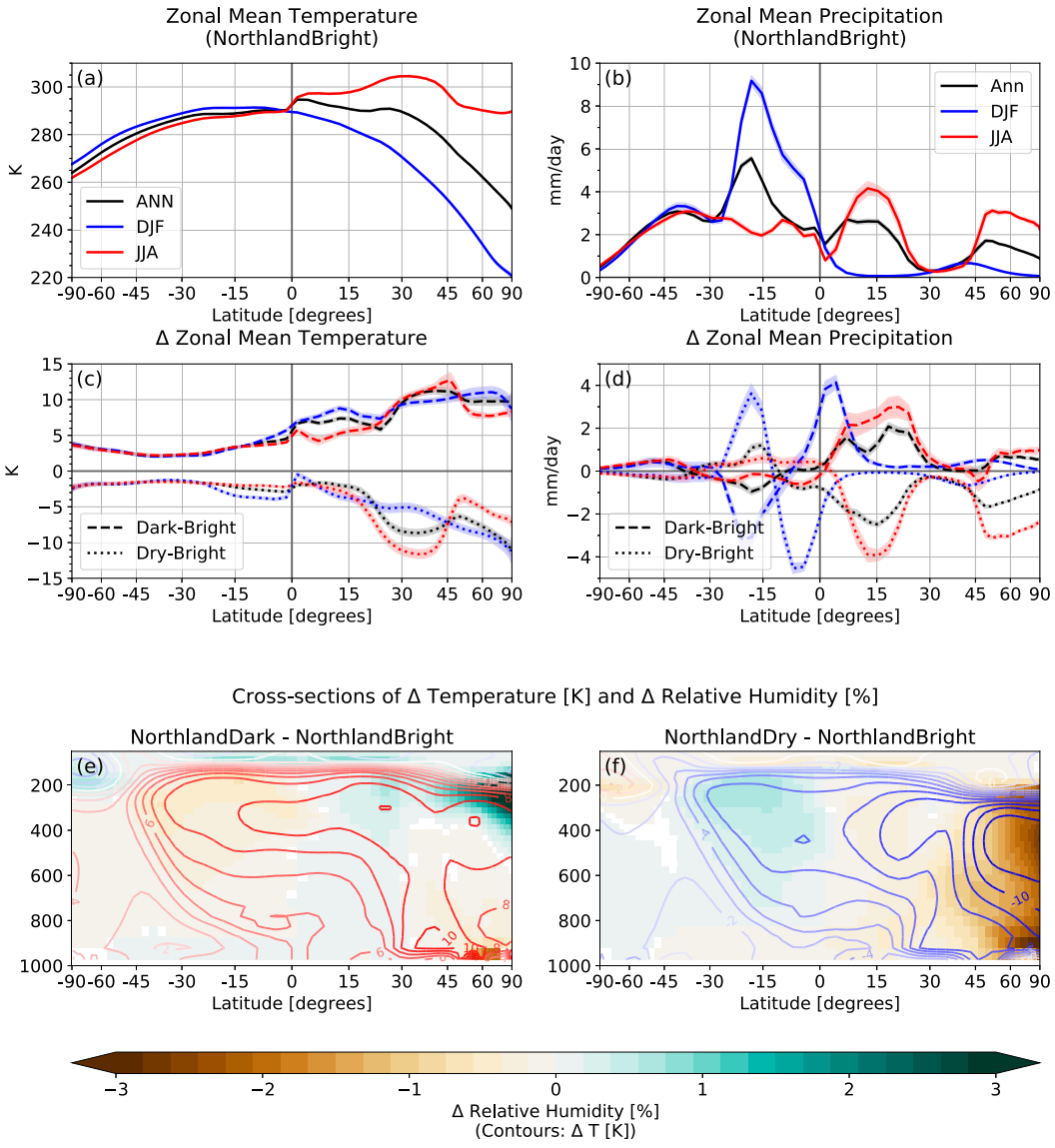

FIG. 2. Zonal mean (a),(c) temperature and (b),(d) precipitation. The NorthlandBright simulation is shown in (a) and (b) (solid lines). The anomalies for NorthlandDark − NorthlandBright (dashed lines) and NorthlandDry − NorthlandBright (dotted lines) are shown in (c) and (d). In (a)–(d), black lines indicate annual mean values, while blue (red) show values for December–February (June–August) in (a) and (c) and cyan (magenta) show values for February–April (August–October) in (b) and (d). Shading in (a)–(d) indicates ±1 standard deviation. Also shown is the annual mean change in zonal mean relative humidity (shading) and temperature (contours) for (e) NorthlandDark-NorthlandBright and (f) NorthlandDry-NorthlandBright. Temperature contours (red/blue lines in (e) and (f) are spaced at 1 K, with red values > 0 and blue values < 0. Only humidity values in (e) and (f) that differ significantly ($p < 0.05$ using Student's t test) are shown.

months of August–October, when the ITCZ is shifted to the north in NorthlandDark versus NorthlandBright (Figs. 2d and 4a,d).

c. *Climate impacts of reduced terrestrial evaporation*

NorthlandDry is the same world as NorthlandBright, except that evaporation from the land surface is suppressed. With all else held equal (i.e., the same amount of incoming energy to the land surface, etc.), this reduction in evaporation from the land surface is expected to lead to greater surface temperatures. This is because if evaporative cooling is reduced, the energy absorbed by the surface must be emitted in the form of sensible heat or longwave radiation, both of which require an increase in surface temperatures. Indeed, both Shukla and Mintz (1982) and Laguë et al. (2019) find that reducing evaporation from the land surface leads to surface warming over land.

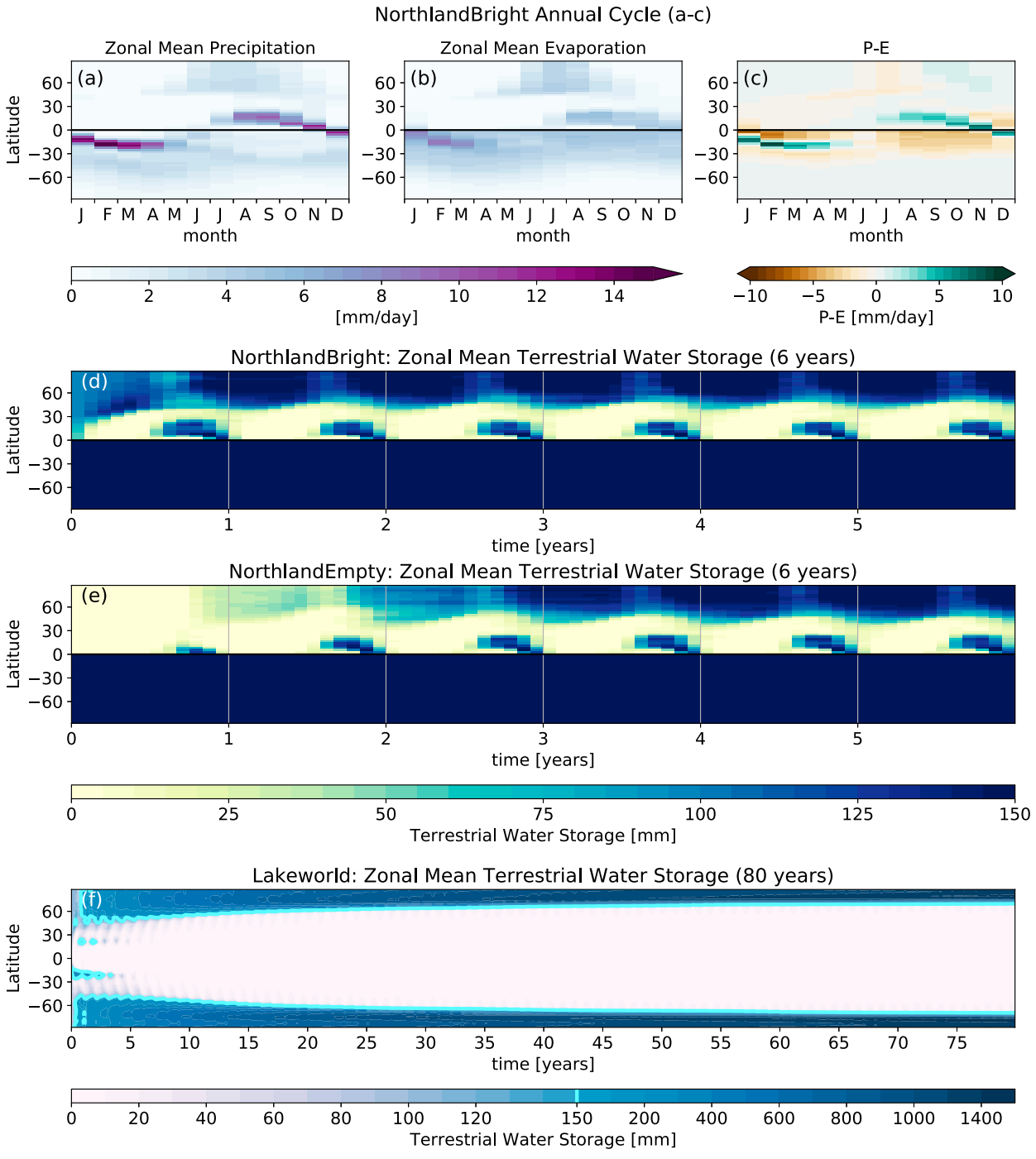

FIG. 3. Zonal mean seasonal cycle of (a) precipitation, (b) evaporation, and (c) precipitation − evaporation ($P - E$) for the spun-up NorthlandBright simulation; the equator/continental boundary is marked by the solid black line. Zonal mean terrestrial water storage over the first 6 simulation years for (d) NorthlandBright and (e) NorthlandEmpty. Zonal mean terrestrial water storage for (f) the full 80-yr simulation of Lakeworld (note the nonlinear color bar). The cyan contour in (f) at 150 mm shows the bucket capacity (i.e., fully saturated soil moisture).

Contrary to previous studies, we find that suppressing evaporation over Northland leads to cooler, not warmer, surface temperatures. Annual mean temperatures in NorthlandDry are 3.2 K cooler globally, and 4.9 K cooler over land than NorthlandBright (Fig. 2c; see also Table S1). The cold anomaly is fairly homogeneous over the ocean hemisphere, but is at its greatest during JJA in the northern subtropics (Fig. 2c). This is surprising as the latent heat flux over land is greatly reduced in

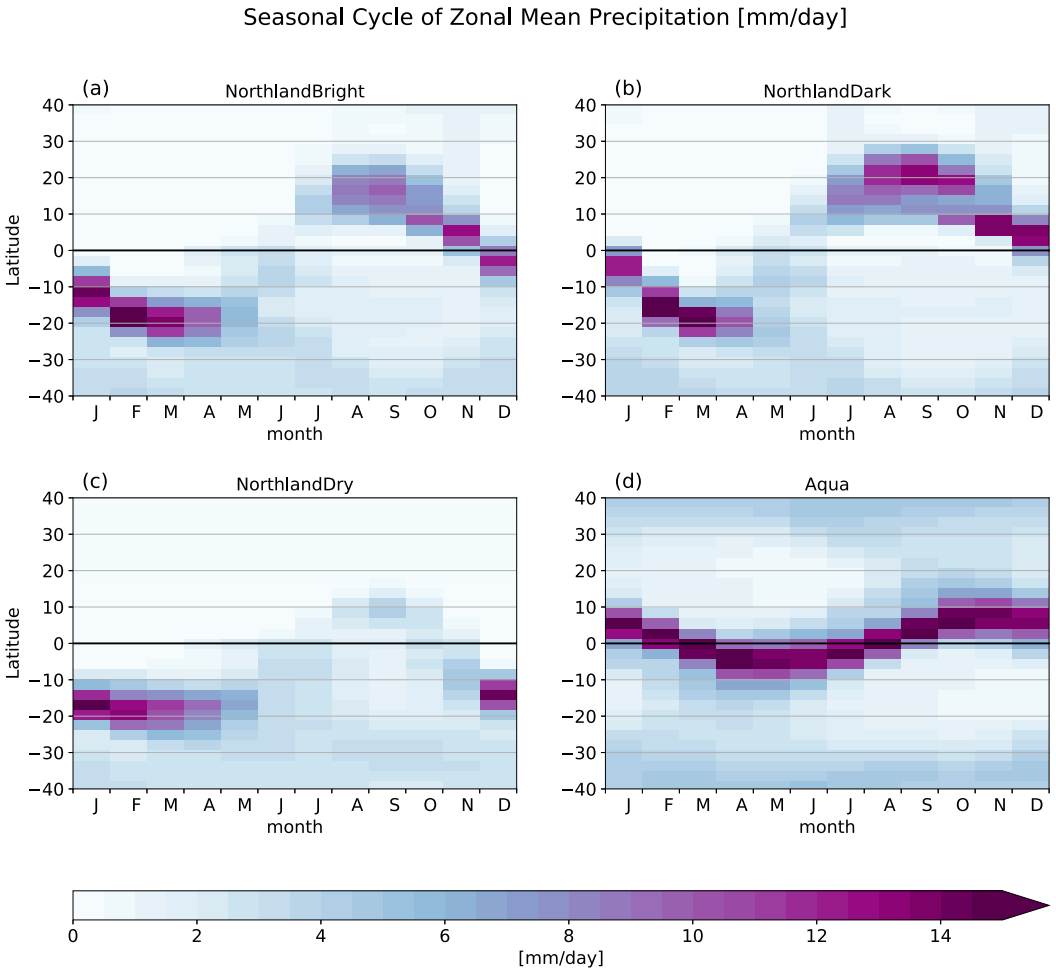

FIG. 4. Seasonal cycle of zonal mean precipitation from 40°S to 40°N in (a) NorthlandBright, (b) NorthlandDark, (c) NorthlandDry, and (d) Aqua.

NorthlandDry compared to NorthlandBright (Fig. 5e), which we would expect to lead to warming. However, suppressing terrestrial evaporation also reduces the amount of water vapor released to the atmosphere over terrestrial regions. Water vapor is a strong greenhouse gas, and if atmospheric water vapor is depleted in sufficiently large quantities, the reduction in the amount of longwave radiation absorbed by the atmosphere and re-emitted down toward the surface would cause net cooling. Moreover, while the direct warming effect of reducing latent cooling is locally isolated to the region where evaporation is reduced, the cooling associated with reduced atmospheric water vapor is much broader in spatial extent, as the atmosphere can mix water vapor (or air with reduced water vapor) beyond the locations where terrestrial evaporation was reduced.

The decrease in atmospheric water vapor (Fig. 2f) due to reduced evaporation from the land surface cools NorthlandDry relative to NorthlandBright by reducing downwelling longwave radiation (Fig. 5a). This reduction in downwelling longwave radiation greatly exceeds the reduction in latent heat flux (which on its own would lead to warming). The reduction in downwelling longwave radiation reaches 150 $W m^{-2}$ in the northern high latitudes, while the reduction in latent heat flux peaks at around 80 $W m^{-2}$, with the largest reductions in the northern tropics and high latitudes (cf. Figs. 5a and 5e). In the dry subtropics, the latent heat flux is already near zero for most of the year in NorthlandBright, so suppressing evaporation has little impact on temperature in this region (Fig. 5e). Hence, cooling is strongest in the dry subtropics, particularly during JJA (Fig. 2c), because the cooling due to the reduction in downwelling longwave from reduced atmospheric water vapor has no warming offset from local reductions in latent cooling. There is actually a slight increase in net shortwave radiation absorption at the surface over land during NH summer months due to reduced absorption of shortwave radiation by water vapor (Fig. 5b). However, the decrease in the downward emission of longwave radiation from reduced atmospheric water vapor dominates the change in absorbed surface energy (Fig. 5f).

At the TOA, there is a substantial reduction in net energy absorbed over the continent from June to August, and an increase in net energy absorbed at the TOA over the continent

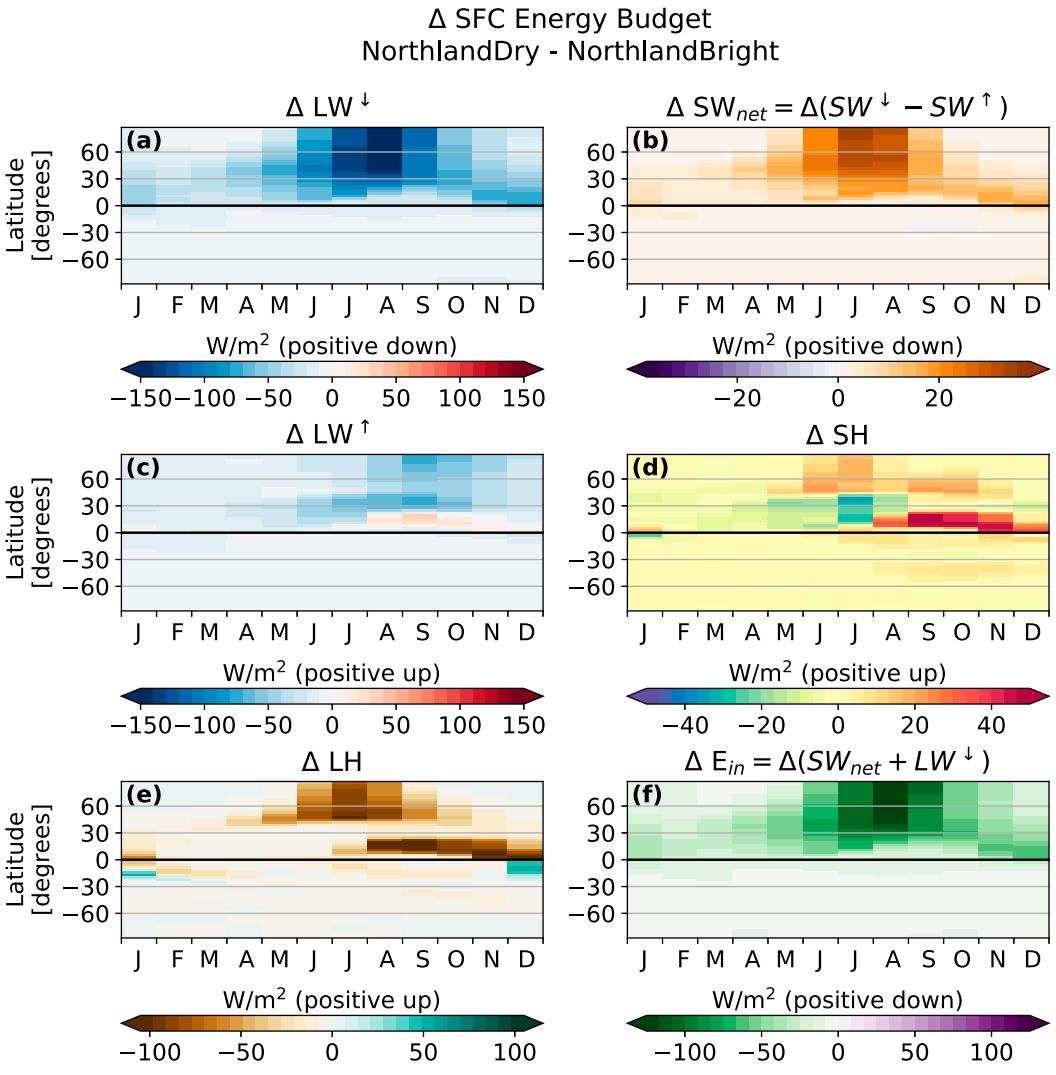

FIG. 5. Change in the zonal mean surface energy budget for NorthlandDry − NorthlandBright over the course of the year. (a) Change in downward LW. (b) Change in net SFC SW. (c) LW emitted by the surface. (d) Sensible heat. (e) Latent heat. (f) The change in net surface energy uptake ($E_{in} = SW^{\downarrow} - SW^{\uparrow} + LW^{\downarrow}$), where positive values indicate more energy into the surface; in the annual mean this would be balanced by $E_{out} = LW^{\uparrow} + LH + SH$.

from September to December (Fig. 6c). These changes are dominated by the change in TOA LW. During NH summer, more LW is lost from the TOA as a result of a smaller greenhouse effect, and there is less net SW absorption due to reduced atmospheric water vapor (Fig. 6). That is, despite the surface being colder during JJA in NorthlandDry than NorthlandBright, there is still more LW lost from the TOA in NorthlandDry because of the reduced greenhouse effect. This contrasts with the driver of changes in TOA LW from September to December, when there is overall more energy absorbed at the TOA in NorthlandDry than NorthlandBright (Fig. 6c). From September to December, NorthlandDry has less LW emission from the TOA, reflecting the overall colder conditions in NorthlandDry compared to NorthlandBright (Fig. 6b).

We can compare the change in land surface temperature over Northland due to suppressed terrestrial evaporation to an equivalent change in albedo, if we assume that land surface temperatures scale linearly with land surface albedo [as was found by Laguë et al. (2019)]. The surface temperature change between NorthlandDark and NorthlandBright implies a 9.9-K increase in land surface temperatures per 0.1 decrease in land surface albedo for our idealized planet (see Table S1). We note that this is much larger than the roughly 2-K increase in surface temperatures per 0.1 decrease in land surface albedo found in Laguë et al. (2019), for a realistic continental configuration in a more complex model. However, intuitively this value should vary with total land area, land distribution, and cloud cover (which is not represented in this model), as modifying land

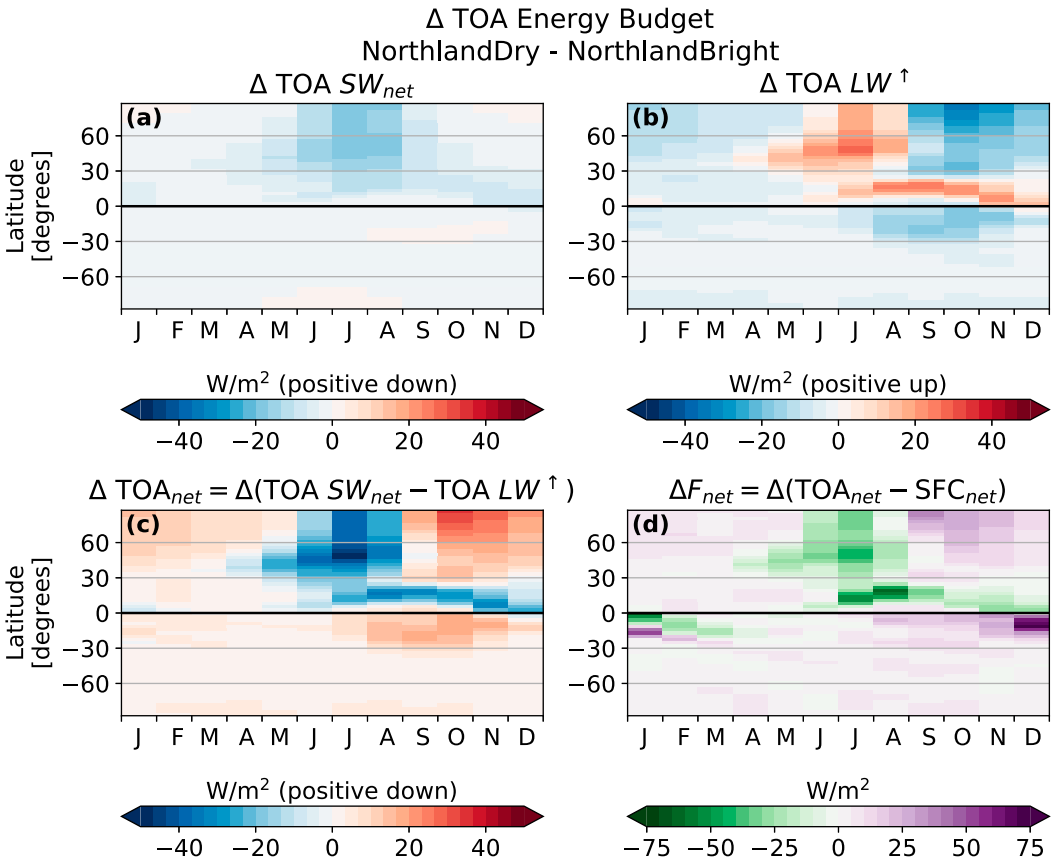

FIG. 6. Change in the zonal mean TOA energy budget for NorthlandDry − NorthlandBright over the course of the year. (a) The change in net TOA SW. (b) The change in outgoing longwave radiation. (c) The net TOA energy budget. (d) The change in the atmospheric energy source F_{net} = TOA_{net} − SFC_{net}, where positive indicates more energy into the atmosphere.

albedo will have a different impact on absorbed SW energy and surface temperatures depending on the presence of clouds and the location of the albedo change. Moreover, surface albedo changes are largely attenuated by the atmosphere on Earth and in more complex models (Donohoe and Battisti 2011); as such, the 0.1 change in surface albedo between NorthlandBright and NorthlandDark results in a much larger change in planetary albedo in Isca than a similar surface albedo change on the real Earth. Applying the 9.9 K per 0.1 decrease in albedo relationship for Northland to the temperature change in NorthlandDry versus NorthlandBright tells us that suppressing terrestrial evaporation over Northland has the equivalent effect on land surface temperatures as increasing the NH albedo by 0.05 (roughly 14%, 0.05/0.35).

The response of precipitation to suppressed terrestrial evaporation in the NorthlandDry experiment is widespread. In particular, precipitation over the continent decreases almost to zero during August–October, which is the wettest part of the year in NorthlandBright. A very weak ITCZ generates a small amount of precipitation over the southern edge of the continent in August–October (Fig. 4c), whereas precipitation is very low over the rest of the continent year round. We note that the structure of the Hadley cell during JJA in NorthlandDry differs from the Hadley cell of the other simulations presented here (Fig. S3). NorthlandDry does not have a large source of moisture over the land surface in the tropics. The ITCZ is very weak during JJA (Fig. 4c), and rather than an overturning circulation driven by the release of latent heat, the circulation is driven by direct thermal heating of the surface. The result is two overturning cells stacked on the equator during JJA, with the lower cell circulating anticlockwise and the upper cell circulating clockwise (Fig. S3f).

d. *Temperature response to suppressed evaporation in various continental configurations*

The unexpected cooling of Northland with suppressed terrestrial evaporation is due to the reduction in downward LW from reduced atmospheric water vapor (and thus a weaker greenhouse effect) dominating any surface warming from reduced latent heat fluxes. Because the Northland continental configuration has no oceanic water source in the NH, NH atmospheric water vapor becomes significantly depleted (Fig. 7o). We further explore the effects of suppressing terrestrial evaporation on surface temperature by considering

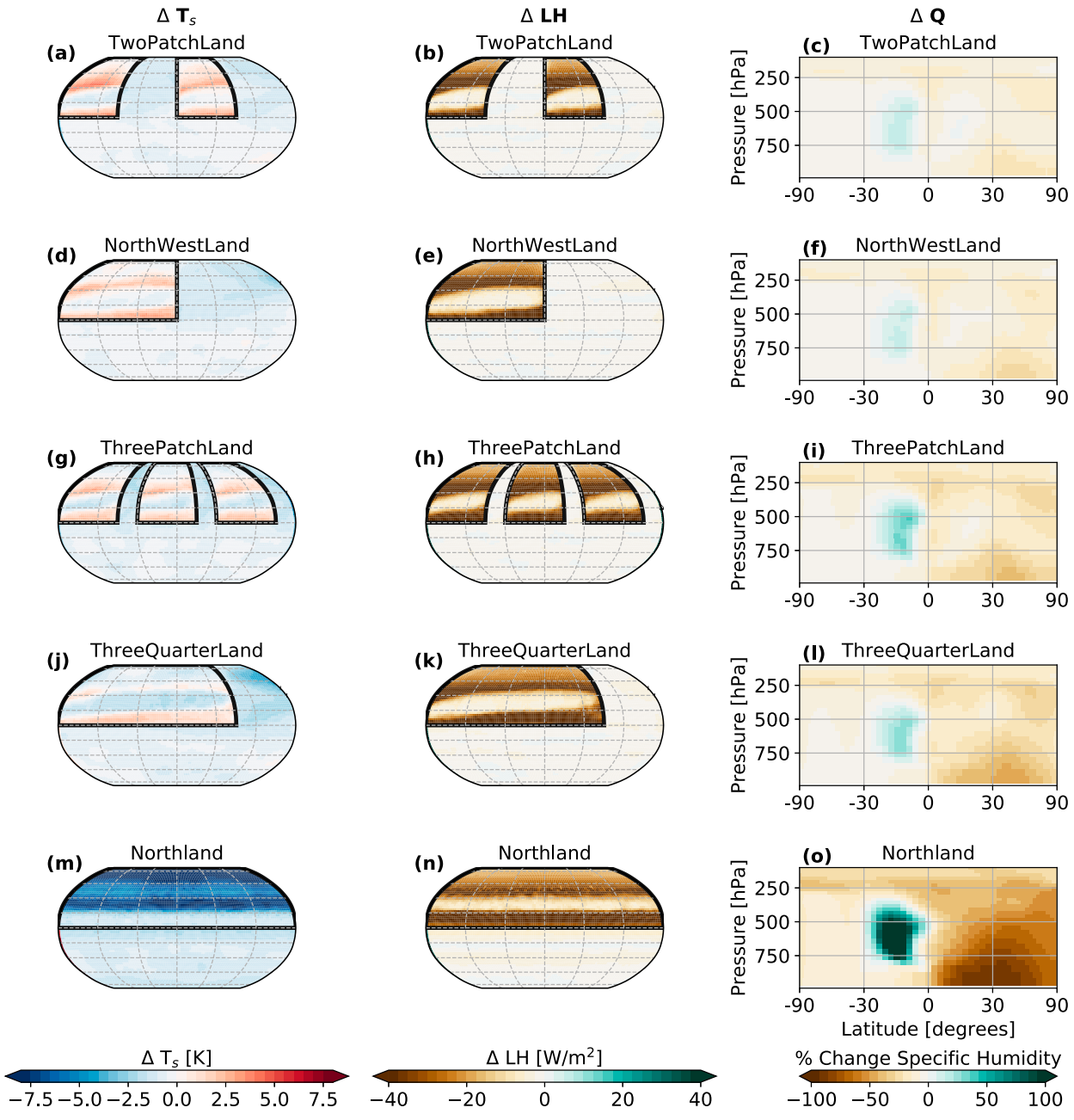

FIG. 7. Annual mean change in (left) surface temperature and (center) latent heat flux, and (right) percent change in zonal mean specific humidity for suppressing terrestrial evaporation in various continental configurations. Thick black lines show the continental boundary.

four additional continental configurations with varying amounts of ocean in the NH: TwoPatchLand, ThreePatchLand, NorthWestLand, and ThreeQuarterLand (Fig. 1, Table 1). We compare simulations where the continents have the same land surface properties as NorthlandBright (i.e., "normal" land surface properties) to simulations where the continents have the same land surface properties as NorthlandDry (i.e., terrestrial evaporation is suppressed), to explore the trade-off between warming from reduced surface latent heat flux and cooling from reduced atmospheric water vapor.

In TwoPatchLand, suppressing terrestrial evaporation leads to 1.0 K of warming over land, on average (Figs. 7a and 8a).

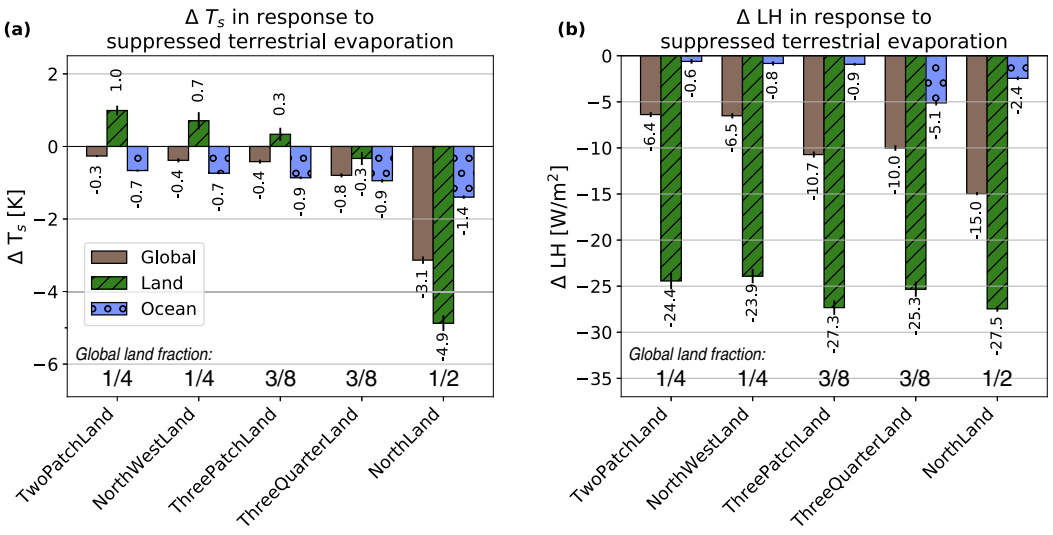

FIG. 8. The area-weighted annual mean change in (a) surface temperature and (b) latent heat flux globally (gray), over land only (green), and over the ocean only (blue), for each continental configuration. Small vertical black lines on each bar indicate one standard deviation. The magnitude of the temperature/latent heat flux change is noted above or below each bar. The total global land fraction for each simulation is noted along the bottom of each panel.

However, as with the dry regions of NorthlandBright, suppressing evaporation over regions that are climatologically dry in TwoPatchLand (i.e., the subtropics) does not lead to any direct warming through reduced evaporative cooling (Fig. 7a). Instead, these subtropical land areas experience cooling when terrestrial evaporation is suppressed as a result of decreased downward LW from reduced atmospheric water vapor. In NorthWestLand, suppressing evaporation also generally leads to warming over land, with an average warming of 0.7 K over land (Figs. 7b and 8a). The warming is not as strong in NorthWestLand as in TwoPatchLand when evaporation is suppressed (Fig. 7a), despite both continental configurations having the same total land area and the same latitudinal distribution of land area, with half of the NH covered by land. The warming is smaller in NorthWestLand despite a comparable (indeed, slightly smaller) reduction in terrestrial latent heat flux (Fig. 8b).

ThreePatchLand and ThreeQuarterLand have the same total land area: in both cases 3/4 of the NH are covered by land. However, suppressing terrestrial evaporation leads to warming of the land for ThreePatchLand, and cooling of the land for ThreeQuarterLand (Fig. 8a). The warming of 0.3 K over land in ThreePatchLand is smaller than in TwoPatchLand or NorthWestLand, reflecting the larger reduction in atmospheric water vapor (Fig. 7i) driven by more land area. In ThreeQuarterLand, the reduction in atmospheric water vapor is large enough to dominate warming from reduced latent heat flux, resulting in net land cooling of 0.3 K (Figs. 7j,l and 8a). The reduction in latent heat flux from land is larger in ThreePatchLand than ThreeQuarterLand, but the reduction in latent heat flux from the ocean is much larger in ThreeQuarterLand than in ThreePatchLand (Fig. 8b). The differences between ThreePatchLand and ThreeQuarterLand (and TwoPatchLand and NorthWestLand) demonstrate that it is not only land area, but also continent size and distribution that modulate the temperature response to suppressed terrestrial evaporation.

The change in terrestrial latent heat flux due to suppressed evaporation over land (Fig. 8b) is approximately equal to the latent heat flux from the simulations with "normal" surface properties (from NorthlandBright), because there is almost no evaporation in the simulations with NorthlandDry land surface properties. The single large continents have slightly lower latent heat fluxes in the so-called normal simulations than their patchy counterparts; that is, TwoPatchLand and ThreePatchLand have slightly larger terrestrial latent heat fluxes than NorthWestLand and ThreeQuarterLand, respectively, and thus have slightly larger changes in latent heat flux from land when terrestrial evaporation is suppressed.

However, we note that the average area-weighted change in latent heat flux from the land surface is of comparable magnitude across all the continental configurations considered here (Fig. 8b), while total reduction in terrestrial latent heat flux scales with total land area. For simulations with the same total land area (e.g., TwoPatchLand and NorthWestLand), the total reduction in terrestrial latent heat flux is similar, but the surface temperature response differs. The temperature change driven by suppressing terrestrial evaporation is greater when the contiguous continental area is larger. This occurs because the atmosphere becomes more depleted in water vapor over a single large continent than it does over two smaller continents separated by ocean. Thus the water vapor cooling effect is stronger over larger continents than smaller ones, even if the direct warming due to reduced latent cooling of the surface is similar.

Over the oceans, surface temperatures cool and evaporation is reduced as a result of suppressing terrestrial evaporation in all the TwoPatchLand, ThreePatchLand, NorthWestLand,

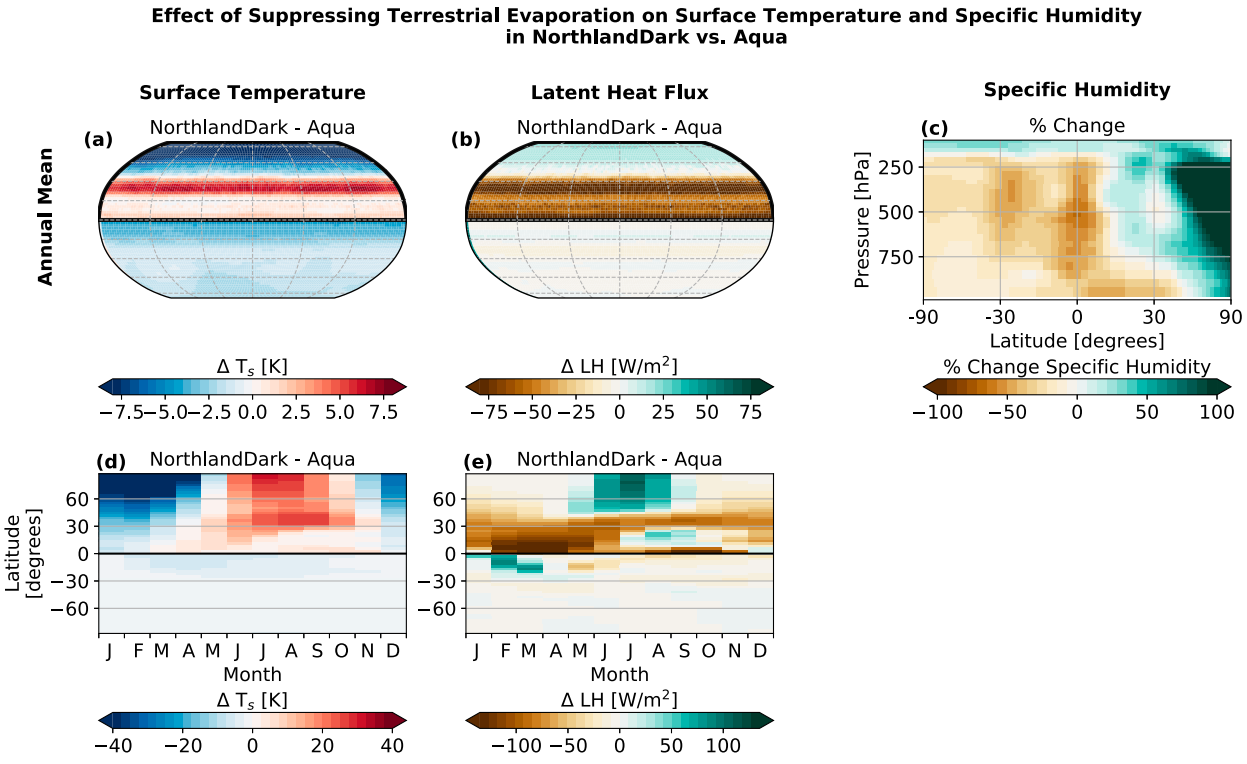

FIG. 9. (left) Change in surface temperature, (center) change in latent heat flux, and (right) percent change in zonal mean specific humidity between NorthlandDark and Aqua, showing (a)–(c) the annual mean change and (d),(e) the zonal-mean seasonal cycle.

ThreeQuarterLand, and Northland continental configurations (Fig. 7). The changes in latent heat flux from the ocean (blue bars in Fig. 8b) must be the result of changes in the local oceanic surface energy budget, mainly over the NH ocean. For example, cooling over the NH ocean in ThreeQuarterLand is more intense than it is over the NH ocean in ThreePatchLand (Fig. 7g vs Fig. 7j), which is consistent with a greater reduction in oceanic latent heat flux in ThreeQuarterLand versus ThreePatchLand. Despite Northland showing the greatest surface cooling and the greatest global reduction in latent heat flux, the reduction in oceanic latent heat flux in Northland is small compared to the other continental configurations (Fig. 8b). This reflects the fact that most of the temperature change in Northland occurs over the land hemisphere, and not over the ocean. In the other continental configurations, much of the reduction in oceanic latent heat flux occurs over the NH, where the temperature changes and decreases in atmospheric water vapor are greatest (Fig. 7). The cooling over the ocean is due to a reduction in atmospheric water vapor from suppressed terrestrial evaporation leading to reductions in downward LW. In turn, cooling over the ocean reduces evaporation from the ocean due to the Clausius–Clapeyron relationship. This generates a weak negative feedback on the ocean temperature, but also further reduces the water vapor flux to the atmosphere. Only in a few ocean regions do we see a slight increase in evaporation (not shown), as might be expected if drier air was being advected off the continent. However, these regions are not all located downstream of the continents; most of the ocean shows a decrease in evaporation due to a reduced greenhouse effect.

We can also consider differences between NorthlandDark and Aqua, as the NH in NorthlandDark has the same albedo as Aqua but a limited capacity to hold water. On the one hand, one might expect the NH land surface in NorthlandDark to be warmer than in Aqua because of limited water available for evaporation (thus potentially less latent cooling of the surface). On the other hand, reduced atmospheric water vapor in the NH of NorthlandDark compared to Aqua could result in cooling (due to a weaker greenhouse effect). In the comparison of NorthlandDark to Aqua however, we are not simply considering differences in water availability; the different NH heat capacities in NorthlandDark and Aqua also lead to differences in evaporation and surface temperatures. The smaller heat capacity over the land surface in NorthlandDark results in a much larger seasonal cycle in surface temperatures, with hotter summers and cooler winters (Fig. 9d). The difference in heat capacity also generates big differences in NH evaporation between NorthlandDark and Aqua, since the available energy at the surface in NorthlandDark is used not only to heat the surface, but also to evaporate water (Figs. 9b,e). In NH summer, high surface temperatures cause a high vapor pressure deficit. Combined with the low heat capacity that requires more energy to be lost by the land surface as heat or moisture, this drives larger latent heat fluxes from the high-latitude land in NorthlandDark than in Aqua, despite Aqua having effectively unlimited water to evaporate. Moreover, the larger

seasonal cycle in temperature in NorthlandDark versus Aqua has a nonlinear effect on evaporation; the atmospheric demand for water vapor increases exponentially with temperature following the Clausius–Clapeyron relationship such that at the same relative humidity the vapor pressure deficit of warmer air is larger than that of cooler air (Hartmann 1994; Bonan 2016). In the annual mean, the tropics in NorthlandDark are hotter and have lower latent heat fluxes than Aqua, while in the high latitudes surface temperatures are lower and evaporative fluxes are higher. This results in an atmosphere that is drier over the NH in the low latitudes, but actually less dry over the NH high latitudes in NorthlandDark than Aqua (Fig. 9c). This is notably different from the TwoPatchLand, ThreePatchLand, NorthWestLand, and ThreeQuarterLand simulations, but is driven primarily by differences in the heat capacity of land versus ocean, rather than differences in water availability/evaporation.

In summary, we find that suppressing terrestrial evaporation has a direct local warming effect on the region of evaporative suppression, by reducing latent cooling of the land surface. However, suppressing terrestrial evaporation indirectly cools globally by reducing atmospheric water vapor (a strong greenhouse gas). In the case of TwoPatchLand, NorthWestLand, and ThreePatchLand, the local warming effect dominates the response in most terrestrial regions, while the dominant effect over ocean and desert land regions is cooling associated with decreased atmospheric water vapor (Fig. 8a). However, when evaporation is suppressed over ThreeQuarterLand and Northland, the atmospheric water vapor effect dominates resulting in cooler surface temperatures over the oceans and most land areas (Fig. 8a). Because Northland does not have any ocean in the Northern Hemisphere, the atmosphere can become much more depleted in water vapor than it can in the other continental configurations (Fig. 7o). In TwoPatchLand, NorthWestLand, and ThreePatchLand, atmospheric water vapor is depleted over the continents, but is replenished over the ocean at all latitudes, such that the zonal-mean reduction in atmospheric water vapor is much less than the water vapor reduction in Northland (Fig. 7, right column). While the reduction in atmospheric water vapor is not as large in ThreeQuarterLand as in Northland, it is large enough for the mean response of land temperatures to be an overall cooling (Figs. 7j and 8a). We deduce that the land surface temperature response to reduced terrestrial evaporation is a function of both total land area (which controls the reduction in terrestrial latent heat flux) and contiguous continent size (which controls how dry the atmosphere becomes).

e. *The role of moisture transport*

In all the Northland simulations except NorthlandDry (which cannot store water on land), a Great Northern Swamp forms in the northern high latitudes. In the absence of a large low-latitude water source, is the Great Northern Swamp sustainable? Here we use an all-land simulation, Lakeworld, to show that the existence of the Great Northern Swamp relies on atmospheric moisture transport from the SH ocean in all other Northland experiments. Lakeworld has no ocean; land surface properties are similar to those in NorthlandBright except that lakes of arbitrary depth are allowed to form on all grid cells, if precipitation exceeds evaporation.

Lakeworld rapidly forms two lakes, one over each pole (Fig. 3f), which deepen as the simulation progresses. Within a few years, all of the water on Lakeworld—which is initialized with 100 mm of water in every grid cell—has been transported to the polar high latitudes, and the land in the tropics is completely dry year-round. The lake edges retreat poleward quickly over the first 35 years, then more slowly as the simulation progresses.

In effect atmospheric circulation redistributes water to concentrate it in the polar regions. On the present-day Earth, the lower branch of the Hadley circulation transports moisture equatorward, but in Lakeworld the moisture is rapidly mixed poleward by midlatitude eddies, then trapped too far poleward for this mechanism of equatorward transport. The atmosphere of Lakeworld is very dry, with atmospheric moisture isolated to the lower troposphere near the summer pole (Fig. S4). Because the atmosphere in Lakeworld is so dry, the greenhouse effect is very weak, causing Lakeworld to be much colder than the simulations that include some ocean (Figs. S1 and S5). Surface temperatures in Lakeworld are above the freezing point year round in the lower latitudes, and at higher latitudes during summer (Fig. S5).

The polar lake in Lakeworld has a much smaller latitudinal extent than the Great Northern Swamp in the Northland simulations. In the Northland experiments, the southern portion of the Great Northern Swamp receives moisture (which is ultimately from the SH ocean) from midlatitude eddies. This does not occur in Lakeworld, because moisture is trapped at the poles after the first few years of the simulation. The lake continues to drift poleward over the course of the Lakeworld simulation. The Lakeworld simulation would have to be run to equilibrium to determine how far poleward the polar lake will retreat. However, we do not continue the Lakeworld simulation beyond 80 years as 1) the extent of the polar lake in equilibrium is not the focus of this study and 2) the atmosphere in an all-land configuration leaks moisture in the current configuration of Isca (Fig. S6). We also explore an all-land simulation that cannot form lakes (i.e., it has the same land surface properties as NorthlandBright). Like Lakeworld, that simulation also quickly transports water to the poles, but because runoff is discarded when soil moisture exceeds the bucket capacity, the simulation rapidly loses water from the system (not shown).

f. *Land's influence on ITCZ location*

The presence of the Northland continent alters the source of energy to the atmosphere by altering the net surface flux of SW (both through surface albedo and changes in water vapor), altering LW absorption in the atmosphere by modulating atmospheric water vapor, and modifying the seasonal timing of energy absorption and release by the land surface. We find that the ITCZ in both the NH and SH of all Northland experiments extends farther poleward than in Aqua (with the exception of NorthlandDry, which has very little precipitation over land), despite the greater water vapor content in the tropics in Aqua (Figs. 4 and 10e). Less SW is absorbed at the NH surface in

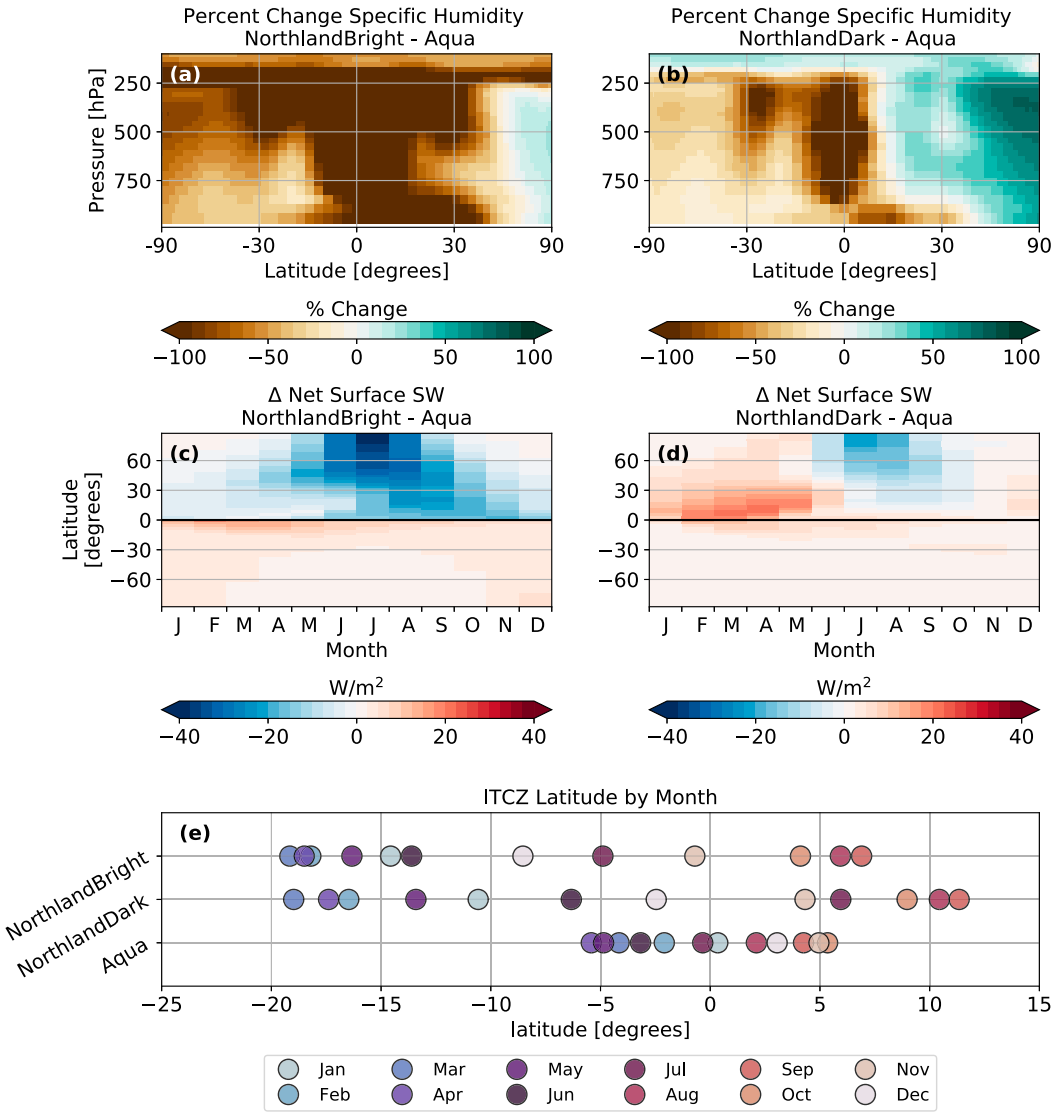

FIG. 10. (top) Zonal mean percent change in annual mean specific humidity for (a) NorthlandBright − Aqua and (b) NorthlandDark − Aqua. (middle) Seasonal cycle of the zonal mean change in net SW absorbed at the surface for (c) NorthlandBright − Aqua and (d) NorthlandDark − Aqua. (e) ITCZ latitude calculated as the center of mass of zonal mean precipitation from 30°S to 30°N for NorthlandBright, NorthlandDark, and Aqua, where each dot represents a single month of the year.

NorthlandBright compared to Aqua because of the high land albedo in NorthlandBright (Fig. 10c). Except in the northern high latitudes, the atmosphere in NorthlandBright has less water vapor than the atmosphere in Aqua (Fig. 10a). NorthlandDark has more water vapor over the NH than Aqua as a result of the higher air temperatures (Fig. 10b). Although the albedo of the NH is identical in NorthlandDark and Aqua, differences in atmospheric water vapor between the simulations result in changes to the amount of SW reaching the surface (Fig. 10d). The presence of the NorthlandDark continent also results in an ITCZ extending farther poleward than both Aqua and NorthlandBright in the NH (Fig. 10e). To explain the ITCZ position as a result of the Northland continent in these experiments, we discuss the differences in the hemispheric energy imbalance between our simulations below.

There is an extensive literature exploring how hemispherically asymmetric sources of energy to the atmosphere cause the atmosphere to transport energy from the energy-rich hemisphere to the energy-poor hemisphere, with a corresponding shift in the zonally averaged ITCZ toward the energy-rich hemisphere (Kang et al. 2008; Yoshimori and Broccoli 2008; Fasullo and Trenberth 2008; Donohoe et al. 2013; Geen et al. 2020). The relationship between the magnitude of cross-equatorial energy transport and the location of the ITCZ has been explored for the modern Earth system, where the ITCZ shifts 2.4°–2.7°S per petawatt increase in northward

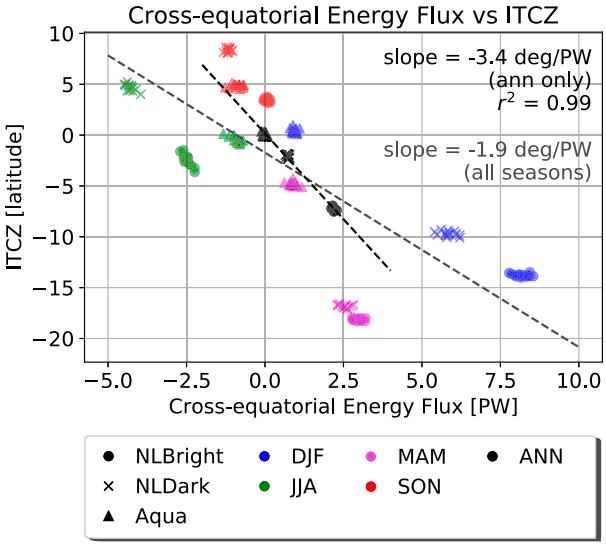

FIG. 11. Relationship between the latitude of the ITCZ and the magnitude of cross-equatorial energy flux. The latitude of the ITCZ is calculated as the center of mass of precipitation between 30°S and 30°N; the magnitude of cross-equatorial energy flux is calculated as the magnitude of meridional atmospheric energy transport at the equator. Black markers indicate annual mean values, while blue, purple, green, and red markers indicate DJF, MAM, JJA, and SON averages, respectively. Circles show values for NorthlandBright, x marks for NorthlandDark, and triangles for Aqua. Each individual marker shows the seasonally averaged value for a single year of the time series. NorthlandDry is not included in the regression calculations here as the ITCZ effectively collapses over the continent.

cross-equatorial energy transport (Donohoe et al. 2013). In our idealized simulations, we find a marginally steeper relationship than Donohoe et al. (2013), with a 3.4° southward shift in the annual mean ITCZ latitude per petawatt increase in northward cross-equatorial energy transport (Fig. 11; see also Fig. S7). Several factors impact this slope, including the gross moist stability of the model and the influence of cloud cover, a mechanism that is absent from our experimental framework (Geen et al. 2020; Voigt et al. 2014).

The greater poleward extent of the zonally averaged ITCZ location is best explained by comparing the NorthlandDark and Aqua experiments, since these two configurations have the same surface albedo and differ only in the heat capacity and capacity to store water in the NH. We argue that the primary reason for the greater poleward extent of the ITCZ in the Northland simulations is the difference in heat capacity between the land and ocean hemispheres, which generates greater hemispheric energy imbalances than in Aqua, both seasonally and in the annual mean.

The lower heat capacity of the NH in NorthlandDark provides less of a buffer to the atmospheric energy imbalance by storing less energy in the surface relative to Aqua during JJA, and releasing less energy during DJF (cf. SFC in Figs. 12f, 12h, 12j, and 12l). During JJA, the ITCZ extends farther poleward over the NH in NorthlandDark than Aqua because the land surface takes up little energy, resulting in a larger atmospheric energy source F_{net} = TOA − SFC in NorthlandDark than Aqua (Geen et al. 2020). During DJF, the ITCZ extends farther poleward over the SH in NorthlandDark than Aqua because the land surface releases little energy, while in Aqua the ocean releases stored energy to the atmosphere; thus, the NH atmosphere is more energy-poor in NorthlandDark than Aqua during DJF. The net effect is that the NH atmospheric energy source is much larger in NorthlandDark than Aqua during JJA, while the NH atmospheric energy source is more negative during DJF in NorthlandDark than Aqua (cf. F_{net} in Figs. 12f,h,j,l; see also Table S2).

In the annual mean, NorthlandDark has a hemispheric imbalance in F_{net}, while F_{net} is symmetric about the equator in Aqua (Table S2). This hemispheric energy imbalance results in an annual mean transport of energy across the equator from the SH to the NH, consistent with a zonally averaged ITCZ sitting south of the equator (Fig. 11). Corresponding to this hemispheric atmospheric energy imbalance, the ITCZ in NorthlandDark extends much farther poleward than the ITCZ in Aqua, both seasonally and in the annual mean. In NorthlandBright and NorthlandDry, the ITCZ extends slightly farther south than in NorthlandDark during DJF because the lower surface albedo (NorthlandBright) and lower water vapor (NorthlandDry) reduces the total amount of energy taken up during NH summer and subsequently released in NH winter by the land surface, accentuating the hemispheric imbalance in the atmospheric energy source that already exists as a result of the smaller heat capacity of land versus ocean (Figs. 12a,c; Table S2). Details of the calculations used for Figs. 11 and 12 are provided in the supplement.

4. Discussion

a. *Temperature response to suppressed terrestrial evaporation*

With all else held equal, reducing evaporation from the land surface should lead to surface warming, as the energy formerly used to evaporate water is instead repartitioned into sensible heat or emitted longwave radiation. While reducing evaporation from the land surface directly leads to warming (Shukla and Mintz 1982; Laguë et al. 2019), reducing water flux from the land surface also impacts atmospheric concentrations of water vapor, a strong greenhouse gas. Given the competing effects of reduced evaporative cooling, which would lead to warming, and reduced longwave trapping by atmospheric water vapor, which would lead to cooling, we hypothesize that a crossing point exists in the temperature response to suppressed land evaporation (Fig. 13). Starting from a state of sufficient atmospheric moisture, reducing evaporation from the land surface should initially lead to surface warming as a result of decreased evaporative cooling of the land surface (regime i in Fig. 13). However, as atmospheric water vapor concentration decreases, the strength of the atmospheric greenhouse effect also decreases, inducing a cooling effect on the surface; the warming signal from suppressed evaporation competes with the cooling from a reduced greenhouse effect (regime ii in

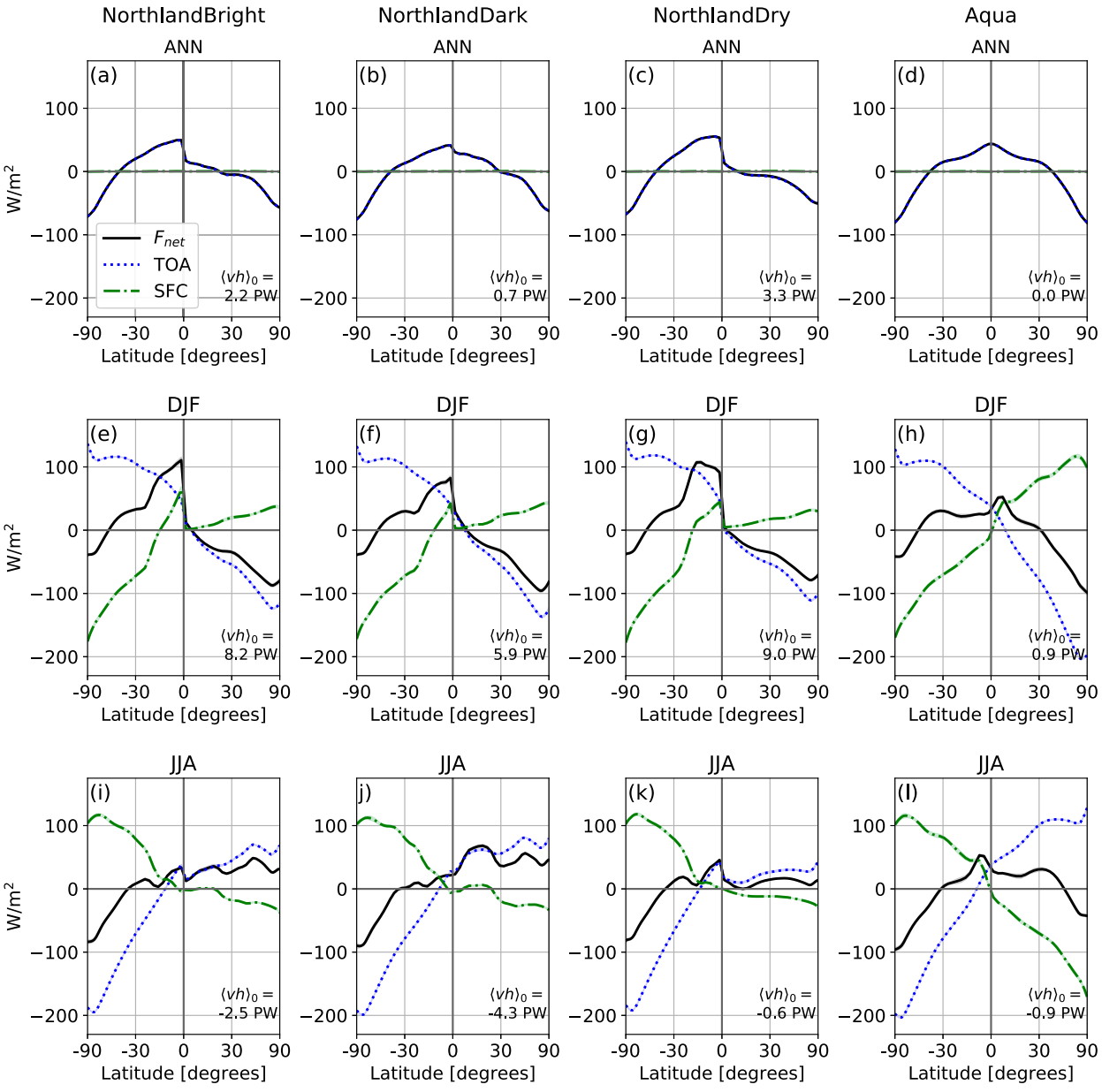

FIG. 12. Zonally averaged net TOA energy flux (TOA; blue dotted line), net surface energy flux (SFC; green dash-dotted line), and the atmospheric column energy source (F_{net} = TOA − SFC; black solid line) for the (top) annual mean, (middle) DJF, and (bottom) JJA. Shown are (a),(e),(i) NorthlandBright, (b),(f),(j) NorthlandDark, (c),(g),(k) NorthlandDry, and (d),(h),(l) Aqua. The total column integrated cross-equatorial atmospheric energy transport (positive northward) for each season is noted in the lower right of each panel.

Fig. 13). Once atmospheric concentrations of water vapor are sufficiently low, the cooling effect from the reduced atmospheric greenhouse effect dominates the surface temperature response (regime iii in Fig. 13).

From our simulations, suppressing evaporation over TwoPatchLand would fit into regime i, where reduced evaporation warms the land surface. NorthWestLand falls between regimes i and ii, where the direct warming effect of reduced evaporation is weaker than in TwoPatchLand, and thus the total warming is more strongly damped by the reduction in atmospheric water vapor. ThreePatchLand and ThreeQuarterLand bracket the crossing point of the temperature response (regime ii), with ThreePatchLand warming slightly and ThreeQuarterLand cooling slightly. Northland falls firmly into regime iii, where any direct warming of the surface is more than outweighed by cooling from reduced atmospheric water vapor. Generally, larger total land areas fall farther to the right on this curve; however, for the same total land area (e.g., TwoPatchLand vs NorthWestLand), the continental arrangement with the larger contiguous continent size falls farther to the right. This

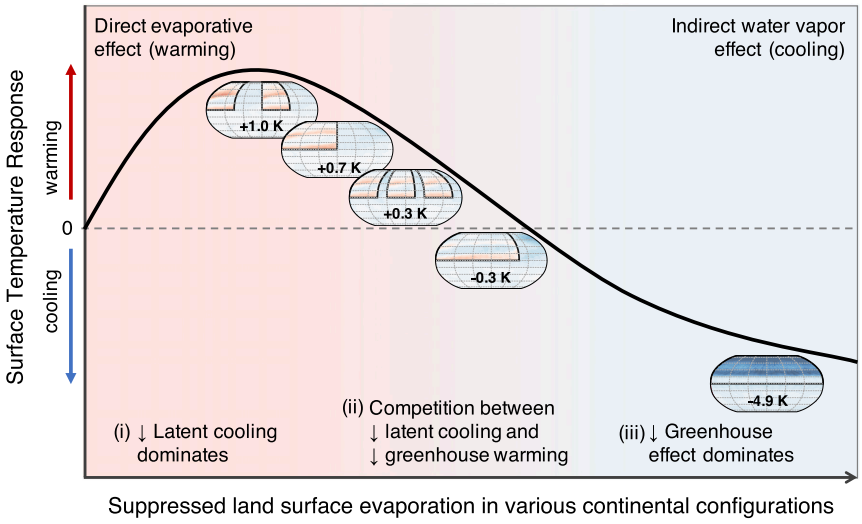

FIG. 13. Schematic showing the surface temperature response to suppressed terrestrial evaporation for a variety of NH continental configurations. Land area generally increases from left to right, although for a given total land area, larger continents sit farther to the right on the curve than smaller, more numerous continents. Qualitative locations of suppressing terrestrial evaporation on TwoPatchLand, NorthWestLand, ThreePatchLand, ThreeQuarterLand, and Northland are shown by the maps of temperature change for each continental configuration, with the annual mean change in land surface temperature noted on each map.

occurs because when the continents are broken up, the atmosphere can be replenished with water vapor when it passes over the ocean, while in the case of a larger contiguous continent, the atmosphere becomes more depleted in water vapor. We suggest the present-day continental configuration of Earth falls into regime i, both because the present-day continental configuration of Earth most closely resembles TwoPatchLand (i.e., there is ample ocean at every latitude) and because previous modeling studies (e.g., Shukla and Mintz 1982; Laguë et al. 2019) found that reducing terrestrial evaporation leads to surface warming over land. Indeed, the largely zonal flow of the atmosphere would shift any continental configuration with ocean at each latitude toward regime i, as the mixing of dry continental and moist oceanic air would prevent any individual latitude from becoming overly depleted in water vapor.

In our simulations, suppressing terrestrial evaporation in all of our continental configurations leads to cooling over the ocean. This differs from the results of Laguë et al. (2019), who found that reduced evaporation with a realistic present-day continental configuration leads to surface warming over most of the ocean.[1] Differences in the ocean temperature response between Laguë et al. (2019) and this study could be due to nuances in circulation due to the use of realistic continental geometry and orography in that study, as well as different intensities of suppressed terrestrial evaporation. In particular, our idealized Isca simulations do not have any representation of cloud cover, and cloud responses to changes in terrestrial evaporation can have large climate feedbacks (Laguë et al. 2019). Reduced terrestrial evaporation can lead to drying of the boundary layer and a reduction in low cloud cover over land, which in turn increases absorbed SW at the surface and drives warming in water-limited systems, while changes in terrestrial evaporation can also lead to cloud changes over ocean regions (Laguë et al. 2019; Kim et al. 2020). Understanding how the presence of clouds and the response of clouds to reduced terrestrial evaporation modify the temperature response to reduced terrestrial evaporation both on land and globally requires future study.

Based on our results from TwoPatchLand/ThreePatchLand versus NorthWestLand/ThreeQuarterLand (section 3d), we postulate that suppressing terrestrial evaporation in continental configurations with large amounts of arid land (e.g., polar continents) would have a much weaker impact on water vapor than continents with moist climates (e.g., in the tropics) and thus would not generate strong large-scale cooling. We also note that we have tested an extreme level of reduced terrestrial evaporation here. We do not consider the response of temperature to smaller reductions in terrestrial evaporation such as those driven by the closure of plants' stomata in response to increased atmospheric CO_2, which have been shown to generate terrestrial warming across CMIP5 and CMIP6 models (Zarakas et al. 2020).

We have explored the temperature response to suppressing terrestrial evaporation over idealized NH continents; in doing so, we have demonstrated that continental configuration is of utmost importance in controlling the temperature response to suppressed terrestrial evaporation. We have identified the

[1] The Shukla and Mintz (1982) study does not inform on changes over the ocean because they prescribe a fixed SST.

competing effects of suppressing terrestrial evaporation on surface temperature without any complicating factors driven by cloud responses. These idealized simulations do not represent cloud cover, and thus do not capture either how the presence of clouds may modulate the surface temperature response to reduced terrestrial evaporation or how cloud changes in response to reduced terrestrial evaporation may further influence surface temperatures, both locally over land and over the ocean. Further study is required to identify the seasonality of this response, which continental configurations lead to warming versus cooling, what level of reduction in continental evaporation is required for warming versus cooling, and what role clouds play in modulating the temperature response to reduced terrestrial evaporation.

b. *Connections to Snowball Earth*

Our results raise the question of how past continental configurations and distributions of water and vegetation on those continents may have impacted both terrestrial and global paleoclimate through water vapor feedbacks. What is the distribution of continents that is required such that decreasing evapotranspiration from the land surface leads to a cooling rather than warming? In present-day Earth, the greenhouse effect is due mainly to water vapor, and the source of water vapor is net evaporation in the tropics (equatorward of 35° latitude), which is distributed globally by the atmospheric circulation. In our TwoPatchLand and NorthWestLand continental configurations, suppressing terrestrial evaporation results in global-scale cooling through reduced atmospheric water vapor, although the land surface generally warms due to reduced latent cooling. However, in our Northland continental configuration, the continent covers the entire hemisphere, which severely reduces the evapotranspiration of water vapor poleward of the ITCZ in the NH. Further reducing terrestrial evaporation in the NorthlandDry experiment reduces the greenhouse effect and causes cooling. In this regard, it is illuminating to consider the Snowball Earth events: global glaciations during which ice covered the entire surface of the Earth (Kirschvink 1992; Hoffman et al. 1998). There is evidence for two such events during the Neoproterozoic between 630 and 750 million years ago, and one in the early Paleoproterozoic 2.5 billion years ago (Abbot et al. 2013; Hoffman et al. 2017), when most of the continental landmasses were located in the tropics (see Kump et al. 2004; Worsley and Kidder 1991, and references therein).

The Snowball Earth atmosphere is cold and holds little moisture (Voigt et al. 2011; Hoffman et al. 2017). Past work suggests that paleogeographic continental configurations cause a reduction in atmospheric water vapor compared to an aquaplanet without continents, increasing direct heating by decreasing cloud cover (Fiorella and Poulsen 2013). Future work could test the robustness of this result and probe whether past tropical megacontinents were large enough to cause a sufficient reduction in tropical water vapor to cool the tropics and contribute to the onset of Snowball events (although the dry atmosphere of Snowball Earth is attributed to the cold temperatures and not vice versa; Voigt et al. 2012; Hoffman et al. 2017). This reduction in tropical water vapor would cause even greater cooling in the extratropics as a consequence of reduced atmospheric energy transport (Rose et al. 2014). If this occurred, cooling by reduced total tropical evaporation would help explain why Snowball Earth happened. However, reductions in continental precipitation would reduce the rate of silicate weathering, thus allowing for greater CO_2 buildup in the atmosphere, which would act against the formation of a Snowball Earth event. In addition, past tropical supercontinent configurations would have had some ocean at each latitude band, more closely resembling our NorthWestLand or ThreeQuarterLand simulations than our Northland simulations. Notably, the NorthWestLand and ThreeQuarterLand configurations bracket the transition from warming to cooling when land evaporation is suppressed, suggesting this process could be relevant for Pangea-like continental configurations, although we have not explored the effect of varying the position (e.g., moving the whole continent to the tropics) of the megacontinent here.

We note that our NorthlandDry simulation has a similar JJA Hadley cell structure as Snowball Earth. The lack of moisture on the land surface in NorthlandDry means that over the continent during NH summer, as in Snowball Earth, the Hadley circulation is dominated by dry dynamics and produces a much smaller overturning circulation than in the present climate (Voigt et al. 2012; Voigt 2013).

c. *Precipitation*

In our Northland simulations, we find that the poleward extent of the ITCZ over the ocean hemisphere is influenced by the existence of the NH continent. Specifically, we find that the small heat capacity and lower water vapor concentrations of the NH lead to the ocean hemisphere ITCZ extending much farther poleward than it does in an aquaplanet simulation. This is similar to the findings of Bordoni and Schneider (2008) and Wei and Bordoni (2018) that ITCZs in aquaplanets with shallower slab oceans extend farther poleward due to stronger energy gradients between the summer and winter hemispheres. Our Northland simulations also demonstrate the importance of hemispheric asymmetries in surface heat storage.

Previous studies have shown how hemispheric energy imbalances drive shifts in the zonal mean location of the ITCZ (e.g., Chiang and Bitz 2005; Broccoli et al. 2006; Kang et al. 2008; Swann et al. 2012; Maroon et al. 2016). In the current continental configuration on Earth, zonal mean changes are not generally representative of regional precipitation change (Byrne and O'Gorman 2015; Kooperman et al. 2018; Atwood et al. 2020). However, given our zonally symmetric continental distribution in Northland, the energy balance framework is a useful tool for understanding the seasonal cycle of circulation and the distribution of precipitation.

In Earth's present-day continental configuration, roughly 68% of the total landmass is in the NH while the remaining 32% is in the SH. This work raises the question of how much the present-day continental configuration impacts the ITCZ location via asymmetries in seasonal heat storage between the hemispheres.

The present study ties into previous work exploring the impact of continental landmasses on the climate system. The

tropical rain belts with an annual cycle and a continent model intercomparison project (TRACMIP; Voigt et al. 2016) showed that the presence of an idealized tropical continent spanning 45° in longitude generally leads to a decrease in global-mean surface temperatures compared to an aquaplanet in several different GCMs. The authors noted that while this cooling might be expected from the increase in planetary albedo, the patterns of change are more complex and probably related to changes in cloud cover. Voigt et al. (2016) used a ''jello'' continent, which is essentially a patch of thin (lower heat capacity) ocean with higher albedo and reduced evaporation. In contrast to our study, there is no limit on water availability for evaporation over the so-called jello continent, which would be equivalent to unlimited soil moisture in our experiments. Simulations with jello continents in an Earth-like configuration generally capture the present-day climate well (Geen et al. 2018; Thomson and Vallis 2019), but might be too idealized for studying precipitation change in response to CO_2 forcing in some tropical regions such as the Amazon basin (Pietschnig et al. 2019). While the reduction in evaporation due to the presence of land leads to cooling in TRACMIP, similar to what we see from Aqua to NorthlandDark or from NorthlandBright to NorthlandDry, the mechanisms for the cooling are different. First, clouds are not modeled in Isca but are noted to have an impact of surface temperature patterns in TRACMIP. Second, the inability of the jello continent to dry out makes the ''warming due to reduced latent cooling'' (regime i in Fig. 13) less extreme, although at the same time the reduction in atmospheric water vapor—which would lead to cooling (regime iii in Fig. 13)—would be expected to be less drastic than in our study.

d. Relationship to all-land planets

Our Lakeworld simulation rapidly transports all the surface water to the poles. We expect this is because the climatological equator-to-pole temperature gradient ensures an even greater gradient in moisture (via the Clausius–Clapeyron relationship), and atmospheric storms transport water vapor toward the high latitudes where the vapor condenses and precipitates. The condensate remains at the poles because evaporation is greatly reduced by the cooling resulting from the reduced greenhouse effect. During summer, some of the high-latitude soil moisture evaporates, but is locally recycled. In the absence of an efficient mechanism to transport moisture from the poles toward the equator, all the moisture ends up accumulating in the polar regions. This ''leaking'' of moisture from the tropics to the poles warrants further study: for example, how much water does the system require to maintain a moist tropics? What controls the latitudinal extent of the polar lake? This distribution of surface water is similar to that on other planets, such as Mars, which has two polar ice caps (Boynton et al. 2002; Wordsworth 2016; Feldman et al. 2004). While the mechanism by which the water on Mars is concentrated in its polar regions is unclear (Wordsworth 2016), we note that this is an intriguing similarity with our all-land simulation.

The presence of large topographical features could potentially modify the distribution of water on a land planet, as it could favor the formation of lakes via runoff into basins rather than at the poles. The distribution of the lakes would then be controlled by surface topography rather than atmospheric moisture transport alone, as is the case in our simulations. Indeed, previous studies of all-land planets that include overland river-like mechanisms to bring water back from the high latitudes to the low latitudes have high soil moisture outside of the polar regions and precipitation maxima in the midlatitude storm tracks (e.g., Kalidindi et al. 2018), unlike our Lakeworld simulation, which has soil moisture maxima at the poles. In their land-planet simulation, Kalidindi et al. (2018) find two distinct climate states in the absence of a seasonal cycle, one hot and dry and one cold and wet; including a seasonal cycle only produces a cold and wet state. While our all-land simulation is cold and wet near the poles, the absence of surface water redistribution means that the tropics in our Lakeworld simulation are cold (compared to Aqua or Northland) and dry. Differences between our results and those of Kalidindi et al. (2018) arise from the addition of clouds, zero obliquity, and importantly the resupply of water to low latitudes in their study. We suspect that without the water recycling mechanism and with a seasonal cycle, Kalidindi et al. (2018) would also observe low values of soil moisture and precipitation except very close to the poles.

5. Conclusions

In this study, we use an idealized climate model to study the climate of Northland, a planet with a continent covering the NH and an ocean covering the SH, and several related continental configurations where the NH contains both land and ocean. The physical properties of land on Earth differ from the ocean in several ways, each of which has an effect on the climate system. Land has a limited capacity to hold water, a higher albedo, and a smaller heat capacity than oceans, and evaporation and turbulent energy exchange from the land surface are influenced by properties of vegetation and soils. By conducting a series of simulations where specific properties of the land surface are modified, we test the sensitivity of surface climate and atmospheric circulation to various aspects of the land surface.

The climatology of Northland has a seasonal temperature cycle that is greatly amplified over the land hemisphere, due to the limited heat capacity of the land surface. On the continent, the tropics are seasonally wet; moisture is brought onto the continent from the ocean by the land-falling ITCZ, but the soils dry out during NH winter. From 20° to 40°N, there is a desert region. In the high latitudes, soils are moist year round. There is rain over high-latitude land during NH summer; in contrast, precipitation declines poleward of 45°S in the ocean hemisphere in all seasons. We show that atmospheric moisture transport forms a swampy region in the high latitudes, both in our Northland simulations and over a land-only planet.

Surprisingly, we find that suppressing terrestrial evaporation over the Northland continent leads to global-scale cooling, with particularly large cooling of 4.9 K over the NH continent; this is in contrast to previous studies that find reducing terrestrial evaporation warms the land surface. With all else held equal, decreasing evaporation would lead to warming as the

land surface would have to shed energy through sensible heat or emitted longwave radiation, both of which are a function of surface temperature. However, in our simulations, we find that suppressing terrestrial evaporation reduces atmospheric water vapor concentrations, and in turn decreases the strength of the greenhouse effect. The decrease in the greenhouse effect due to reduced water vapor leads to surface cooling, which outweighs any surface warming resulting directly from reduced evaporative cooling in the Northland continental configuration. Using a series of alternative continental configurations where only part of the NH is covered with land, we demonstrate that there is a trade-off between the local warming effect of reduced latent heat flux and the global cooling effect of reduced atmospheric water vapor. When the NH has two 90°-wide continents separated by ocean, suppressing terrestrial evaporation leads to 1 K of warming over land, while a single 180°-wide NH continent leads to weaker warming of 0.7 K over land. Three equally spaced 90°-wide NH continents lead to even weaker warming of 0.3 K over land, while a single 270°-wide continent leads to cooling of 0.3 K over land. The land only experiences warming as a result of suppressed terrestrial evaporation in regions with soil moisture (i.e., not in the subtropics). Over the oceans, suppressing terrestrial evaporation leads to reduced atmospheric water vapor and decreased downwelling LW, which reduces sea surface temperatures and ocean evaporation, in turn further reducing atmospheric water vapor. We conclude that both globally and over land, the temperature response to suppressed terrestrial evaporation is not only a function of total land area and the latitudinal distribution of land, but also of continent size.

We find that the ITCZ extends much farther poleward, over both the land and ocean hemispheres, in our Northland simulations compared to an aquaplanet simulation. This is primarily the result of the difference in surface heat capacity between the land and ocean hemispheres, which leads to a larger hemispheric imbalance in atmospheric energy in the Northland simulations compared to an aquaplanet.

By exploring the climate of Northland, this study provides insight into the role of hemispheric asymmetries in continental distribution on surface climate and atmospheric circulation, as well as into energetic constraints on the ITCZ location. We have identified a fundamental trade-off in the effect of terrestrial evaporation on surface temperatures that warrants further study. Northland provides an ideal limit for probing fundamental impacts of hemispheric asymmetries and raises new questions about the role of continental distribution, planetary albedo, and terrestrial evaporation in modulating the climate system.

Acknowledgments. We wish to thank the organizers of the 2018 Advanced Climate Dynamics Course, where this project began (https://www.uib.no/en/rs/acdc/118773/acdc-2018-hemispheric-asymmetry-climate). We thank W. R. Boos, A. L. S. Swann, and W. Kang for their helpful discussions and feedback. We acknowledge postdoctoral funding support for MML from the James S. McDonnell Foundation Postdoctoral Fellowship in Dynamic and Multiscale Systems. MP acknowledges funding by the University of Exeter College of Engineering Mathematics and Physical Sciences, and the U.K.–China Research and Innovation Partnership Fund through the Met Office Climate Science for Service Partnership (CSSP) China as part of the Newton Fund. In addition, MP's gratitude is due to the Rupert Ford Award (administered by the Royal Meteorological Society) and the University of Exeter College of Engineering Mathematics and Physical Sciences PhD Mobility Fund, who provided the funding for her research visit to the University of Washington, Seattle, which facilitated collaboration on this project. We thank the editor and three reviewers for their thoughtful, constructive feedback on this manuscript.

Data availability statement. The Isca climate model is publicly available at https://github.com/ExeClim/Isca. The data presented in this paper are archived on Dryad, accessible at https://datadryad.org/stash/dataset/doi:10.6078/D1399Q.

REFERENCES

Abbot, D. S., A. Voigt, D. Li, G. L. Hir, R. T. Pierrehumbert, M. Branson, D. Pollard, and D. D. B. Koll, 2013: Robust elements of Snowball Earth atmospheric circulation and oases for life. *J. Geophys. Res. Atmos.*, **118**, 6017–6027, https://doi.org/10.1002/jgrd.50540.

Atwood, A. R., A. Donohoe, D. S. Battisti, X. Liu, and F. S. R. Pausata, 2020: Robust longitudinally-variable responses of the ITCZ to a myriad of climate forcings. *Geophys. Res. Lett.*, **47**, e2020GL088833, https://doi.org/10.1029/2020GL088833.

Bonan, G. B., 2008: *Ecological Climatology*. Cambridge University Press, 563 pp.

——, 2016: *Ecological Climatology*. 3rd ed. Cambridge University Press, 692 pp., https://doi.org/10.1017/CBO9781107339200.

Bordoni, S., and T. Schneider, 2008: Monsoons as eddy-mediated regime transitions of the tropical overturning circulation. *Nat. Geosci.*, **1**, 515–519, https://doi.org/10.1038/ngeo248.

Boynton, W. V., and Coauthors, 2002: Distribution of hydrogen in the near surface of Mars: Evidence for subsurface ice deposits. *Science*, **297**, 81–85, https://doi.org/10.1126/science.1073722.

Broccoli, A. J., K. Dahl, and R. J. Stouffer, 2006: Response of the ITCZ to Northern Hemisphere cooling. *Geophys. Res. Lett.*, **33**, L01702, https://doi.org/10.1029/2005GL024546.

Budyko, M. I., 1961: The heat balance of the Earth's surface. *Sov. Geogr.*, **2**, 3–13, https://doi.org/10.1080/00385417.1961.10770761.

——, 1969: The effect of solar radiation variations on the climate of the Earth. *Tellus*, **21**, 611–619, https://doi.org/10.3402/tellusa.v21i5.10109.

——, 1974: *Climate and Life*. Academic Press, 507 pp.

Byrne, M. P., and P. A. O'Gorman, 2015: The response of precipitation minus evapotranspiration to climate warming: Why the "wet-get-wetter, dry-get-drier" scaling does not hold over land. *J. Climate*, **28**, 8078–8092, https://doi.org/10.1175/JCLI-D-15-0369.1.

Canadell, A. J., R. B. Jackson, J. R. Ehleringer, H. A. Mooney, O. E. Sala, and E. Schulze, 1996: Maximum rooting depth of vegetation types at the global scale. *Oecologia*, **108**, 583–595, https://doi.org/10.1007/BF00329030.

Cess, R. D., and S. D. Goldenberg, 1981: The effect of ocean heat capacity upon global warming due to increasing atmospheric carbon dioxide. *J. Geophys. Res.*, **86**, 498–502, https://doi.org/10.1029/JC086iC01p00498.

Charney, J. G., 1975: Dynamics of deserts and drought in the Sahel. *Quart. J. Roy. Meteor. Soc.*, **101**, 193–202, https://doi.org/10.1002/qj.49710142802.

Cheng, L., K. E. Trenberth, J. Fasullo, T. Boyer, J. Abraham, and J. Zhu, 2017: Improved estimates of ocean heat content from 1960 to 2015. *Sci. Adv.*, **3**, e1601545, https://doi.org/10.1126/SCIADV.1601545.

Chiang, J. C. H., and C. M. Bitz, 2005: Influence of high latitude ice cover on the marine intertropical convergence zone. *Climate Dyn.*, **25**, 477–496, https://doi.org/10.1007/s00382-005-0040-5.

Cho, M. H., A. R. Yang, E. H. Baek, S. M. Kang, S. J. Jeong, J. Y. Kim, and B. M. Kim, 2018: Vegetation–cloud feedbacks to future vegetation changes in the Arctic regions. *Climate Dyn.*, **50**, 3745–3755, https://doi.org/10.1007/s00382-017-3840-5.

Croll, J., 1870: On ocean-currents. *London Edinburgh Dublin Philos. Mag. J. Sci.*, **39**, 81–106, https://doi.org/10.1080/14786447008640278.

Davin, E. L., and N. de Noblet-Ducoudré, 2010: Climatic impact of global-scale deforestation: Radiative versus nonradiative processes. *J. Climate*, **23**, 97–112, https://doi.org/10.1175/2009JCLI3102.1.

Donohoe, A., and D. S. Battisti, 2011: Atmospheric and surface contributions to planetary albedo. *J. Climate*, **24**, 4402–4418, https://doi.org/10.1175/2011JCLI3946.1.

——, J. Marshall, D. Ferreira, and D. McGee, 2013: The relationship between ITCZ location and cross-equatorial atmospheric heat transport: From the seasonal cycle to the Last Glacial Maximum. *J. Climate*, **26**, 3597–3618, https://doi.org/10.1175/JCLI-D-12-00467.1.

——, K. C. Armour, G. H. Roe, D. S. Battisti, and L. Hahn, 2020: The partitioning of meridional heat transport from the Last Glacial Maximum to CO_2 quadrupling in coupled climate models. *J. Climate*, **33**, 4141–4165, https://doi.org/10.1175/JCLI-D-19-0797.1.

Eliassen, A., and E. Palm, 1960: On the transfer of energy in stationary mountain waves. *Geofys. Publ.*, **22** (3), 1–23.

Fasullo, J. T., and K. E. Trenberth, 2008: The annual cycle of the energy budget. Part II: Meridional structures and poleward transports. *J. Climate*, **21**, 2313–2325, https://doi.org/10.1175/2007JCLI1936.1.

Feldman, W. C., and Coauthors, 2004: Global distribution of near-surface hydrogen on Mars. *J. Geophys. Res. Planets*, **109**, E09006, https://doi.org/10.1029/2003JE002160.

Ferrari, R., and D. Ferreira, 2011: What processes drive the ocean heat transport? *Ocean Modell.*, **38**, 171–186, https://doi.org/10.1016/j.ocemod.2011.02.013.

Fiorella, R. P., and C. J. Poulsen, 2013: Dehumidification over tropical continents reduces climate sensitivity and inhibits snowball Earth initiation. *J. Climate*, **26**, 9677–9695, https://doi.org/10.1175/JCLI-D-12-00820.1.

Forget, G., and D. Ferreira, 2019: Global ocean heat transport dominated by heat export from the tropical Pacific. *Nat. Geosci.*, **12**, 351–354, https://doi.org/10.1038/s41561-019-0333-7.

Geen, R., F. H. Lambert, and G. K. Vallis, 2018: Regime change behavior during Asian monsoon onset. *J. Climate*, **31**, 3327–3348, https://doi.org/10.1175/JCLI-D-17-0118.1.

——, S. Bordoni, D. S. Battisti, and K. Hui, 2020: Monsoons, ITCZs and the concept of the global monsoon. *Rev. Geophys.*, **58**, e2020RG000700, https://doi.org/10.1029/2020RG000700.

Harris, C. R., and Coauthors, 2020: Array programming with NumPy. *Nature*, **585**, 357–362, https://doi.org/10.1038/s41586-020-2649-2.

Hartmann, D. L., 1994: *Global Physical Climatology*. Vol. 56, Academic Press, 411 pp.

Held, I. M., 2005: The gap between simulation and understanding in climate modeling. *Bull. Amer. Meteor. Soc.*, **86**, 1609–1614, https://doi.org/10.1175/BAMS-86-11-1609.

——, P. L. Panetta, and R. T. Pierrehumbert, 1985: Stationary external Rossby waves in vertical shear. *J. Atmos. Sci.*, **42**, 865–883, https://doi.org/10.1175/1520-0469(1985)042<0865:SERWIV>2.0.CO;2.

Hoffman, P. F., A. J. Kaufman, G. P. Halverson, and D. P. Schrag, 1998: A Neoproterozoic Snowball Earth. *Science*, **281**, 1342–1346, https://doi.org/10.1126/science.281.5381.1342.

——, and Coauthors, 2017: Snowball Earth climate dynamics and Cryogenian geology–geobiology. *Sci. Adv.*, **3**, e1600983, https://doi.org/10.1126/sciadv.1600983.

Hoyer, S., and J. Hamman, 2017: xarray: N-D labeled arrays and datasets in Python. *J. Open Res. Software*, **5**, 10, https://doi.org/10.5334/jors.148.

IPCC, 2013: *Climate Change 2013: The Physical Science Basis*. T. F. Stocker et al., Eds, Cambridge University Press, 1535 pp., https://doi.org/10.1017/CBO9781107415324.

Jeevanjee, N., P. Hassanzadeh, S. Hill, and A. Sheshadri, 2017: A perspective on climate model hierarchies. *J. Adv. Model. Earth Syst.*, **9**, 1760–1771, https://doi.org/10.1002/2017MS001038.

Jin, Z., T. P. Charlock, W. L. Smith, and K. Rutledge, 2004: A parameterization of ocean surface albedo. *Geophys. Res. Lett.*, **31**, L22301, https://doi.org/10.1029/2004GL021180.

Kalidindi, S., C. H. Reick, T. Raddatz, and M. Claussen, 2018: Two drastically different climate states on an Earth-like terraplanet. *Earth Syst. Dyn.*, **9**, 739–756, https://doi.org/10.5194/esd-9-739-2018.

Kang, S. M., 2020: Extratropical influence on the tropical rainfall distribution. *Curr. Climate Change Rep.*, **6**, 24–36, https://doi.org/10.1007/S40641-020-00154-Y.

——, I. M. Held, D. M. W. Frierson, and M. Zhao, 2008: The response of the ITCZ to extratropical thermal forcing: Idealized slab-ocean experiments with a GCM. *J. Climate*, **21**, 3521–3532, https://doi.org/10.1175/2007JCLI2146.1.

Kim, J. E., M. M. Laguë, and A. L. S. Swann, 2020: Evaporative resistance is of equal importance as surface albedo in high-latitude surface temperatures due to cloud feedbacks. *Geophys. Res. Lett.*, **47**, e2019GL085663, https://doi.org/10.1029/2019GL085663.

Kirschvink, J. L., 1992: Late Proterozoic low-latitude global glaciation: The snowball earth. *The Proterozoic Biosphere: A Multidisciplinary Study*, Cambridge University Press, 51–52.

Kooperman, G. J., Y. Chen, F. M. Hoffman, C. D. Koven, K. Lindsay, M. S. Pritchard, A. L. S. Swann, and J. T. Randerson, 2018: Forest response to rising CO_2 drives zonally asymmetric rainfall change over tropical land. *Nat. Climate Change*, **8**, 434–440, https://doi.org/10.1038/s41558-018-0144-7.

Kuhlbrodt, T., and J. Gregory, 2012: Ocean heat uptake and its consequences for the magnitude of sea level rise and climate change. *Geophys. Res. Lett.*, **39**, L18608, https://doi.org/10.1029/2012GL052952.

Kump, L. R., J. F. Kasting, and R. G. Crane, 2004: *The Earth System*. 2nd ed., Pearson Prentice Hall, 419 pp.

Laguë, M. M., and A. L. Swann, 2016: Progressive midlatitude afforestation: Impacts on clouds, global energy transport, and precipitation. *J. Climate*, **29**, 5561–5573, https://doi.org/10.1175/JCLI-D-15-0748.1.

——, G. B. Bonan, and A. L. S. Swann, 2019: Separating the impact of individual land surface properties on the terrestrial surface energy budget in both the coupled and uncoupled

land–atmosphere system. *J. Climate*, **32**, 5725–5744, https://doi.org/10.1175/JCLI-D-18-0812.1.

Levins, R., 1966: The strategy of model building in population biology. *Amer. Sci.*, **5**, 420–431.

Loft, G., 1918: The Gulf Stream and the North Atlantic drift. *J. Geog.*, **17**, 8–17, https://doi.org/10.1080/00221341808984367.

Maher, P., and Coauthors, 2019: Model hierarchies for understanding atmospheric circulation. *Rev. Geophy.*, **57**, 250–280, https://doi.org/10.1029/2018RG000607.

Manabe, S., 1969: Climate and the ocean circulation. *Mon. Wea. Rev.*, **97**, 739–774, https://doi.org/10.1175/1520-0493(1969)097<0739:CATOC>2.3.CO;2.

——, and T. B. Terpstra, 1974: The effect of mountains on the general circulation of the atmosphere as identified by numerical experiments. *J. Atmos. Sci.*, **31**, 3–42, https://doi.org/10.1175/1520-0469(1974)031<0003:TEOMOT>2.0.CO;2.

——, R. J. Stouffer, M. J. Spelman, and K. Bryan, 1991: Transient responses of a coupled ocean–atmosphere model to gradual changes of atmospheric CO_2. Part I. Annual mean response. *J. Climate*, **4**, 785–818, https://doi.org/10.1175/1520-0442(1991)004<0785:TROACO>2.0.CO;2.

Maroon, E. A., D. M. Frierson, S. M. Kang, and J. Scheff, 2016: The precipitation response to an idealized subtropical continent. *J. Climate*, **29**, 4543–4564, https://doi.org/10.1175/JCLI-D-15-0616.1.

Marshall, D. P., and L. Zanna, 2014: A conceptual model of ocean heat uptake under climate change. *J. Climate*, **27**, 8444–8465, https://doi.org/10.1175/JCLI-D-13-00344.1.

Marshall, J., and R. A. Plumb, 2007: *Atmosphere, Ocean, and Climate Dynamics: An Introductory Text*. Academic Press, 344 pp.

McFarlane, N. A., 1987: The effect of orographically excited gravity wave drag on the general circulation of the lower stratosphere and troposphere. *J. Atmos. Sci.*, **44**, 1775–1800, https://doi.org/10.1175/1520-0469(1987)044<1775:TEOOEG>2.0.CO;2.

McMullin, E., 1985: Galilean idealization. *Stud. Hist. Philos. Sci.*, **16**, 247–273, https://doi.org/10.1016/0039-3681(85)90003-2.

Milly, P. C. D., and B. Shmakin, 2002: Global modeling of land water and energy balances. Part I: The Land Dynamics (LaD) model. *J. Hydrometeor.*, **3**, 283–299, https://doi.org/10.1175/1525-7541(2002)003<0283:GMOLWA>2.0.CO;2.

Nilsson, J., P. L. Langen, D. Ferreira, and J. Marshall, 2013: Ocean basin geometry and the salinification of the Atlantic Ocean. *J. Climate*, **26**, 6163–6184, https://doi.org/10.1175/JCLI-D-12-00358.1.

North, G. R., J. G. Mengel, and D. A. Short, 1983: Simple energy balance model resolving the seasons and the continents: Application to the astronomical theory of the ice ages. *J. Geophys. Res.*, **88**, 6576–6586, https://doi.org/10.1029/JC088iC11p06576.

Oke, T. R., 1987: *Boundary Layer Climates*. 2nd ed. Routledge, 464 pp., https://doi.org/10.4324/9780203407219

Payne, R. E., 1972: Albedo of the sea surface. *J. Atmos. Sci.*, **29**, 959–970, https://doi.org/10.1175/1520-0469(1972)029<0959:AOTSS>2.0.CO;2.

Pietschnig, M., F. H. Lambert, M. Saint-Lu, and G. K. Vallis, 2019: The presence of Africa and limited soil moisture contribute to future drying of South America. *Geophys. Res. Lett.*, **46**, 12 445–12 453, https://doi.org/10.1029/2019GL084441.

Queney, P., 1948: The problem of air flow over mountains: A summary of theoretical studies. *Bull. Amer. Meteor. Soc.*, **29**, 16–26, https://doi.org/10.1175/1520-0477-29.1.16.

Richardson, P. L., 1980: Benjamin Franklin and Timothy Folger's first printed chart of the Gulf Stream. *Science*, **207**, 643–645, https://doi.org/10.1126/science.207.4431.643.

Rose, B. E. J., K. C. Armour, D. S. Battisti, N. Feldl, and D. D. B. Koll, 2014: The dependence of transient climate sensitivity and radiative feedbacks on the spatial pattern of ocean heat uptake. *Geophys. Res. Lett.*, **41**, 1071–1078, https://doi.org/10.1002/2013GL058955.

Sellers, P. J., and Coauthors, 1996: Comparison of radiative and physiological effects of doubled atmospheric CO_2 on climate. *Science*, **271**, 1402–1406, https://doi.org/10.1126/science.271.5254.1402.

Sellers, W. D., 1969: Global climatic model based on the energy balance of the Earth–atmosphere system. *J. Appl. Meteor.*, **8**, 392–400, https://doi.org/10.1175/1520-0450(1969)008<0392:AGCMBO>2.0.CO;2.

Shukla, J., and Y. Mintz, 1982: Influence of land-surface evapotranspiration on the Earth's climate. *Science*, **215**, 1498–1501, https://doi.org/10.1126/science.215.4539.1498.

Sikma, M., and J. Vilà-Guerau de Arellano, 2019: Substantial reductions in cloud cover and moisture transport by dynamic plant responses. *Geophys. Res. Lett.*, **46**, 1870–1878, https://doi.org/10.1029/2018GL081236.

Stouffer, R. J., S. Manabe, and K. Bryan, 1989: Interhemispheric asymmetry in climate response to a gradual increase of atmospheric CO_2. *Nature*, **342**, 660–662, https://doi.org/10.1038/342660a0.

Sud, Y. C., J. Shukla, and Y. Mintz, 1988: Influence of land surface roughness on atmospheric circulation and precipitation: A sensitivity study with a general circulation model. *J. Appl. Meteor. Climatol.*, **27**, 1036–1054, https://doi.org/10.1175/1520-0450(1988)027<1036:IOLSRO>2.0.CO;2.

Sutton, R. T., B. Dong, and J. M. Gregory, 2007: Land/sea warming ratio in response to climate change: IPCC AR4 model results and comparison with observations. *Geophys. Res. Lett.*, **34**, L02701, https://doi.org/10.1029/2006GL028164.

Swann, A. L. S., I. Y. Fung, and J. C. H. Chiang, 2012: Mid-latitude afforestation shifts general circulation and tropical precipitation. *Proc. Natl. Acad. Sci. USA*, **109**, 712–716, https://doi.org/10.1073/pnas.1116706108.

Thomson, S. I., and G. K. Vallis, 2019: Hierarchical modeling of solar system planets with Isca. *Atmosphere*, **10**, 803, https://doi.org/10.3390/atmos10120803.

Trenberth, K. E., and J. M. Caron, 2001: Estimates of meridional atmosphere and ocean heat transports. *J. Climate*, **14**, 3433–3443, https://doi.org/10.1175/1520-0442(2001)014<3433:EOMAAO>2.0.CO;2.

Vallis, G. K., and Coauthors, 2018: Isca, v1.0: A framework for the global modelling of the atmospheres of earth and other planets at varying levels of complexity. *Geosci. Model Dev.*, **11**, 843–859, https://doi.org/10.5194/gmd-11-843-2018.

Voigt, A., 2013: The dynamics of the Snowball Earth Hadley circulation for off-equatorial and seasonally varying insolation. *Earth Syst. Dyn.*, **4**, 425–438, https://doi.org/10.5194/esd-4-425-2013.

——, D. Abbot, R. Pierrehumbert, and J. Marotzke, 2011: Initiation of a Marinoan snowball Earth in a state-of-the-art atmosphere–ocean general circulation model. *Climate Past*, **7**, 249–263, https://doi.org/10.5194/cp-7-249-2011.

——, I. M. Held, and J. Marotzke, 2012: Hadley cell dynamics in a virtually dry snowball Earth atmosphere. *J. Atmos. Sci.*, **69**, 116–128, https://doi.org/10.1175/JAS-D-11-083.1.

——, S. Bony, J. L. Dufresne, and B. Stevens, 2014: The radiative impact of clouds on the shift of the intertropical convergence zone. *Geophys. Res. Lett.*, **41**, 4308–4315, https://doi.org/10.1002/2014GL060354.

——, and Coauthors, 2016: The tropical rain belts with an annual cycle and a continent model intercomparison project: TRACMIP. *J. Adv. Model. Earth Syst.*, **8**, 1868–1891, https://doi.org/10.1002/2016MS000748.

Wallace, J. M., Y. Zhang, and J. A. Renwick, 1995: Dynamic contribution to hemispheric mean temperature trends. *Science*, **270**, 780–783, https://doi.org/10.1126/science.270.5237.780.

Wei, H.-H., and S. Bordoni, 2018: Energetic constraints on the ITCZ position in idealized simulations with a seasonal cycle. *J. Adv. Model. Earth Syst.*, **10**, 1708–1725, https://doi.org/10.1029/2018MS001313.

Wiscombe, W., and S. Warren, 1980: A model for spectral albedo I: Pure snow. *J. Atmos. Sci.*, **37**, 2712–2733, https://doi.org/10.1175/1520-0469(1980)037<2712:AMFTSA>2.0.CO;2.

Wordsworth, R. D., 2016: The climate of early Mars. *Annu. Rev. Earth Planet. Sci.*, **44**, 381–408, https://doi.org/10.1146/annurev-earth-060115-012355.

Worsley, T. R., and D. L. Kidder, 1991: First-order coupling of paleogeography and CO_2, with global surface temperature and its latitudinal contrast. *Geology*, **19**, 1161–1164, https://doi.org/10.1130/0091-7613(1991)019<1161:FOCOPA>2.3.CO;2.

Yoshimori, M., and A. J. Broccoli, 2008: Equilibrium response of an atmosphere-mixed layer ocean model to different radiative forcing agents: Global and zonal mean response. *J. Climate*, **21**, 4399–4423, https://doi.org/10.1175/2008JCLI2172.1.

Zarakas, C. M., A. L. Swann, M. M. Laguë, K. C. Armour, and J. T. Randerson, 2020: Plant physiology increases the magnitude and spread of the transient climate response to CO_2 in CMIP6 Earth system models. *J. Climate*, **33**, 8561–8578, https://doi.org/10.1175/JCLI-D-20-0078.1.

Zelinka, M. D., D. A. Randall, M. J. Webb, and S. A. Klein, 2017: Clearing clouds of uncertainty. *Nat. Climate Change*, **7**, 674–678, https://doi.org/10.1038/nclimate3402.

Supplemental Information for "Terrestrial evaporation and global climate: lessons from Northland, a planet with a hemispheric continent"

Marysa M. Laguë*

Department of Earth and Planetary Science, University of California Berkeley, Berkeley, CA, USA, and University of Saskatchewan Coldwater Lab, Canmore, Alberta, Canada

Marianne Pietschnig

Department of Mathematics, University of Exeter, Exeter, United Kingdom

Sarah Ragen

School of Oceanography, University of Washington, Seattle, WA, USA

Timothy A. Smith

Oden Institute for Computational Sciences, The University of Texas at Austin, Austin, TX, USA

David S. Battisti

Department of Atmospheric Sciences, University of Washington, Seattle, WA, USA

Corresponding author address: Marysa M. Laguë, Department of Earth and Planetary Science, University of California Berkeley, 307 McCone Hall, Berkeley, CA 94720.

E-mail: mlague@berkeley.edu

1. Hemispheric energy imblance and the location of the Zonal mean ITCZ

a. Definition of the net TOA and SFC energy fluxes

To quantify the excess (or deficit) of energy being absorbed by the atmosphere at any latitude, we calculate the net downward flux of energy at the top of the atmosphere TOA and net downward flux of energy at the surface SFC, and define their difference F_{net} as the atmospheric column energy source:

$$TOA = SW^{\downarrow}_{TOA} - SW^{\uparrow}_{TOA} - LW^{\uparrow}_{TOA} \tag{1}$$

$$SFC = SW^{\downarrow}_{SFC} - SW^{\uparrow}_{SFC} + LW^{\downarrow}_{SFC} - LW^{\uparrow}_{SFC} - SH_{SFC} - LH_{SFC} \tag{2}$$

$$F_{net} = TOA - SFC \tag{3}$$

In equations 1-3, SW, LW, SH, and LH indicate shortwave radiation, longwave radiation, sensible heat, and latent heat, respectively. The sign convention is such that a positive TOA represents energy gained by the atmosphere plus ocean/land, while a positive SFC represents energy gained by the surface. Positive values of F_{net} represent a gain of energy by the atmospheric column, either from the TOA or the surface.

b. Cross-equatorial energy transport

Figure 10 of the main text shows a scatterplot of the location of the ITCZ, defined as the location of the center of mass of precipitation between 30°S and 30°N, and the total atmospheric equatorial energy transport $\langle vh \rangle$ at the equator $\phi = 0$:

$$\langle vh \rangle_0 \;=\; \frac{1}{g}\int_0^{2\pi}\int_{sfc}^{toa} v \times (c_p T + Lq + gz)\ \mathrm{d}\lambda\ \mathrm{dp}\ . \tag{4}$$

In Eq. 4, $h = c_p T + L_v q + gz$ is the moist static energy, v is the meridional wind, T is the temperature of the air, q is water vapor mixing ratio, z is the height, c_p is the heat capacity for dry air, L is

the latent heat of vaporization, and g is the acceleration due to gravity. In the annual mean, cross-equatorial atmospheric energy transport can be diagnosed from the hemispheric asymmetry in F_{net} (Kang et al. 2008; Yoshimori and Broccoli 2008; Fasullo and Trenberth 2008; Donohoe et al. 2013). However, because atmospheric heat storage on sub-annual timescales is non-negligible, we calculate cross-equatorial atmospheric heat transport from the column-integrated meridional transport of moist static energy, both seasonally and in the annual mean in our simulations.

c. Relationship between hemispheric energy balance and the latitude of the ITCZ

The relationship between ITCZ location and cross equatorial energy transport shown in figures 10 and S7 is based on several assumptions that stem from physical arguments/constraints. These are: (i) the overwhelming majority of energy transport is accomplished by the Hadley circulation (Hadley 1735; Pierrehumbert 2002); (ii) the ITCZ is nearly co-located with the rising branch of the Hadley circulation (Dima and Wallace 2003; Bischoff and Schneider 2014); (iii) the efficiency of energy transport by the Hadley circulation is invariant to the climate state (i.e., the gross moist stability is constant; see Neelin and Held (1987); Frierson (2007)); (iv) the ITCZ is nearly co-located with with the position of the Energy Flux Equator (EFE, Kang et al. (2008); Bischoff and Schneider (2014); see below); (v) the cross equatorial energy flux is linearly related to the distance off the equator of the EFE (Bischoff and Schneider 2016); and (vi) that the energy tendency in the atmosphere is small compared to the changes in the net energy F_{net} so that the system is nearly in equilibrium.

These assumptions hold for annual averaged observations and annual average output from climate models run using various boundary conditions, including idealized aquaplanet simulations. We point the reader to Geen et al. (2020) for a review of the theory and the evidence in support of each of these assumptions. Here we only report the degree to which these assumptions hold in our

experiments. An alternative approach proposed by Privé and Plumb (2007) relates the location of the ITCZ to the maximum of near-surface moist static energy rather than to inter-hemispheric energy imbalances (Bordoni and Schneider 2008), but in this work we focus primarily on the effect of land heat capacity on inter-hemispheric energy imbalances.

Not surprisingly, the tropical energy transport in our various continental configurations is overwhelmingly due to the Hadley circulation, and the ITCZ is nearly co-located with the rising branch of the Hadley circulation (assumptions (i) and (ii) respectively; not shown). The tendency in atmospheric energy is generally very small compared to the changes in F_{net} (assumption (vi)).

The EFE is the latitude ϕ where the meridional energy transport $\langle vh \rangle$ is zero. Figure S7b shows the cross equatorial energy flux is linearly related to the location of the EFE (assumption (v), except for some distortion at the solstices in the Northland experiments. Figure S7c shows that in our experiments, the EFE is a fair indicator of the position of the ITCZ (assumption (iv)) in almost all seasons in both the Northland and Aqua experiments; the exception is for summertime in the Northland experiments, when the Hadley circulation is somewhat distorted and there are large changes in gross moist stability, violating assumption (iii). Finally, because the ITCZ is nearly linearly related to the EFE latitude, and the cross equatorial energy transport $\langle vh \rangle_0$ is nearly linearly related to the EFE, the ITCZ should also be linearly related to $\langle vh \rangle$. Figure S7a shows this is roughly true, excepting the summer months in the Northland experiments where the location of the EFE is distorted from the location of the ITCZ.

References

Bischoff, T., and T. Schneider, 2014: Energetic constraints on the position of the Intertropical Convergence Zone. *Journal of Climate*, **27 (13)**, 4937–4951, doi:10.1175/JCLI-D-13-00650.1.

Bischoff, T., and T. Schneider, 2016: The equatorial energy balance, ITCZ position, and double-ITCZ bifurcations. *Journal of Climate*, **29 (8)**, 2997–3013, doi:10.1175/JCLI-D-15-0328.1.

Bordoni, S., and T. Schneider, 2008: Monsoons as eddy-mediated regime transitions of the tropical overturning circulation. *Nature Geoscience*, **1 (8)**, 515–519, doi:10.1038/ngeo248.

Dima, I. M., and J. M. Wallace, 2003: On the seasonality of the Hadley Cell. *Journal of the Atmospheric Sciences*, **60 (12)**, 1522–1527, doi:10.1175/1520-0469(2003)060⟨1522:OTSOTH⟩2.0.CO;2.

Donohoe, A., J. Marshall, D. Ferreira, and D. Mcgee, 2013: The relationship between ITCZ location and cross-equatorial atmospheric heat transport: From the seasonal cycle to the Last Glacial Maximum. *Journal of Climate*, **26 (11)**, 3597–3618, doi:10.1175/JCLI-D-12-00467.1.

Fasullo, J. T., and K. E. Trenberth, 2008: The Annual Cycle of the Energy Budget. Part II: Meridional Structures and Poleward Transports. *Journal of Climate*, **21 (10)**, 2313–2325, doi:10.1175/2007JCLI1936.1.

Frierson, D. M., 2007: The dynamics of idealized convection schemes and their effect on the zonally averaged tropical circulation. *Journal of the Atmospheric Sciences*, **64 (6)**, 1959–1974, doi:10.1175/JAS3935.1.

Geen, R., S. Bordoni, D. S. Battisti, and K. Hui, 2020: Monsoons, ITCZs and the Concept of the Global Monsoon. *Reviews of Geophysics*, 1–45, doi:10.1029/2020rg000700.

Hadley, G., 1735: Concerning the Cause of the General Trade-Winds. *Royal Society of London Philosophical Transactions Series I*, **39**, 58–62.

Kang, S. M., I. M. Held, D. M. W. Frierson, and M. Zhao, 2008: The Response of the ITCZ to Extratropical Thermal Forcing: Idealized Slab-Ocean Experiments with a GCM. *Journal of Climate*, **21 (14)**, 3521–3532, doi:10.1175/2007JCLI2146.1.

Neelin, J. D., and I. M. Held, 1987: Modeling tropical convergence based on the moist static energy budget. 3–12 pp., doi:10.1175/1520-0493(1987)115⟨0003:MTCBOT⟩2.0.CO;2.

Pierrehumbert, R. T., 2002: The hydrologic cycle in deep-time climate problems. *Nature*, **419 (6903)**, 191–198, doi:10.1038/nature01088.

Privé, N. C., and A. R. Plumb, 2007: Monsoon dynamics with interactive forcing. Part I: Axisymmetric studies. *Journal of the Atmospheric Sciences*, **64 (5)**, 1417–1430, doi:10.1175/JAS3916.1.

Yoshimori, M., and A. J. Broccoli, 2008: Equilibrium Response of an Atmosphere-Mixed Layer Ocean Model to Different Radiative Forcing Agents: Global and Zonal Mean Response. *Journal of Climate*, **21 (17)**, 4399–4423, doi:10.1175/2008JCLI2172.1.

LIST OF TABLES

	Area-weighted Surface Temperature [K]					
	NorthlandBright			NorthlandDry		
	global	land	ocean	global	land	ocean
ANN	278.5 ± 0.1	277.1 ± 0.1	279.8 ± 0.0	275.3 ± 0.1	272.2 ±0.2	278.4 ± 0.0
DJF	270.6 ± 0.1	259.3 ± 0.1	282.0 ± 0.1	267.6 ± 0.1	254.9 ± 0.2	280.3 ± 0.1
JJA	285.7 ± 0.1	293.6 ± 0.1	277.9 ± 0.0	282.4 ± 0.1	288.2 ± 0.2	276.6 ± 0.0
	NorthlandDark			Aqua		
	global	land	ocean	global	land	ocean
ANN	283.4 ± 0.0	284.5 ± 0.1	282.2 ± 0.0	284.6 ± 0.0	–	284.6 ± 0.2
DJF	275.5 ± 0.1	266.6 ± 0.1	284.5 ± 0.0	284.6 ±0.0	–	284.6 ± 0.2
JJA	290.4 ± 0.0	300.7 ± 0.1	280.1 ± 0.0	284.6 ± 0.0	–	284.6 ± 0.3
	NorthWestLand			NorthWestLandDry		
	global	land	ocean	global	land	ocean
ANN	281.7 ± 0.1	281.7 ± 0.2	281.7 ± 0.0	281.3 ± 0.0	282.4 ± 0.2	280.9 ± 0.0
DJF	278.8 ± 0.1	268.1 ± 0.3	282.3 ± 0.1	278.1 ± 0.1	267.3 ± 0.3	281.6 ± 0.1
JJA	284.4 ± 0.1	294.4 ± 0.2	281.1 ± 0.0	284.4 ± 0.1	297.0 ± 0.2	280.4 ± 0.0
	PatchyLand			PatchyLandDry		
	global	land	ocean	global	land	ocean
ANN	281.7 ± 0.0	281.7 ± 0.1	281.6 ± 0.0	281.4 ± 0.0	282.7 ± 0.1	281.0 ± 0.0
DJF	279.1 ± 0.0	269.2 ± 0.2	282.2 ± 0.0	278.6 ± 0.0	269.1 ± 0.0	281.6 ± 0.0
JJA	284.1 ± 0.0	293.3 ± 0.1	281.2 ± 0.0	284.2 ± 0.0	295.6 ± 0.2	280.5 ± 0.0

TABLE S1. Average ($\pm 1\sigma$) area-weighted surface temperature for the whole globe, only land areas, and only ocean areas for the annual mean, DJF, and JJA. Temperatures and standard deviations are rounded to the nearest 0.1 K (i.e. ± 0.0 indicates interannual $\sigma < 0.1$ K).

	SH			NH			Hemispheric Imbalance (NH - SH)		
	SFC [PW]	TOA [PW]	F_{net} [PW]	SFC [PW]	TOA [PW]	F_{net} [PW]	Δ SFC [PW]	Δ TOA [PW]	ΔF_{net} [PW]
	ANN								
NLBright	0.07 ± 0.03	2.37 ± 0.03	2.44 ± 0.03	0.09 ± 0.01	-2.26 ± 0.04	-2.16 ± 0.03	0.03 ± 0.03	-4.63 ± 0.05	-4.61 ± 0.06
NLDark	0.06 ± 0.02	0.71 ± 0.04	0.77 ± 0.04	0.10 ± 0.02	-0.58 ± 0.04	-0.47 ± 0.04	0.05 ± 0.02	-1.29 ± 0.08	-1.24 ± 0.07
NLDry	0.06 ± 0.04	3.59 ± 0.02	3.65 ± 0.03	0.11 ± 0.03	-3.49 ± 0.05	-3.38 ± 0.03	0.05 ± 0.05	-7.08 ± 0.06	-7.03 ± 0.06
Aqua	0.03 ± 0.06	0.07 ± 0.03	0.10 ± 0.06	0.02 ± 0.02	0.07 ± 0.04	0.09 ± 0.05	-0.01 ± 0.07	0.00 ± 0.06	-0.01 ± 0.11
	DJF								
NLBright	-15.18 ± 0.15	24.83 ± 0.04	9.65 ± 0.16	4.62 ± 0.12	-15.21 ± 0.07	-10.5 ± 0.14	19.80 ± 0.25	-40.04 ± 0.09	-20.24 ± 0.30
NLDark	-16.56 ± 0.16	23.50 ± 0.03	6.95 ± 0.17	5.28 ± 0.12	-15.27 ± 0.07	-9.99 ± 0.16	21.84 ± 0.24	-38.78 ± 0.08	-16.94 ± 0.31
NLDry	-14.62 ± 0.12	25.57 ± 0.03	10.95 ± 0.12	4.32 ± 0.08	-14.36 ± 0.07	-10.0 ± 0.08	18.94 ± 0.15	-39.93 ± 0.09	-20.99 ± 0.17
Aqua	-19.39 ± 0.08	22.31 ± 0.05	2.92 ± 0.09	19.04 ± 0.13	-21.86 ± 0.04	-2.82 ± 0.13	38.43 ± 0.15	-44.17 ± 0.08	-5.74 ± 0.16
	MAM								
NLBright	7.77 ± 0.14	-4.86 ± 0.03	2.90 ± 0.15	-7.42 ± 0.15	5.93 ± 0.09	-1.49 ± 0.13	-15.18 ± 0.28	10.79 ± 0.11	-4.39 ± 0.25
NLDark	8.33 ± 0.12	-5.99 ± 0.04	2.34 ± 0.12	-7.84 ± 0.09	7.91 ± 0.12	0.07 ± 0.14	-16.17 ± 0.20	13.90 ± 0.15	-2.27 ± 0.24
NLDry	7.10 ± 0.12	-4.22 ± 0.02	2.88 ± 0.12	-7.27 ± 0.09	5.65 ± 0.08	-1.63 ± 0.15	-14.38 ± 0.20	9.87 ± 0.09	-4.51 ± 0.25
Aqua	7.77 ± 0.09	-7.45 ± 0.03	0.32 ± 0.08	-7.35 ± 0.12	7.30 ± 0.08	-0.05 ± 0.13	-15.12 ± 0.17	14.75 ± 0.08	-0.37 ± 0.18
	JJA								
NLBright	17.00 ± 0.08	-19.61 ± 0.05	-2.61 ± 0.11	-3.52 ± 0.05	11.51 ± 0.12	7.99 ± 0.13	-20.52 ± 0.11	31.12 ± 0.16	10.60 ± 0.23
NLDark	17.65 ± 0.08	-21.68 ± 0.07	-4.03 ± 0.09	-3.31 ± 0.05	15.68 ± 0.11	12.37 ± 0.13	-20.96 ± 0.11	37.36 ± 0.16	16.40 ± 0.21
NLDry	16.75 ± 0.03	-18.32 ± 0.02	-1.57 ± 0.05	-3.24 ± 0.08	5.85 ± 0.19	2.61 ± 0.13	-19.99 ± 0.08	24.16 ± 0.21	4.18 ± 0.17
Aqua	19.10 ± 0.11	-21.86 ± 0.05	-2.76 ± 0.13	-19.4 ± 0.08	22.30 ± 0.06	2.90 ± 0.10	-38.50 ± 0.15	44.16 ± 0.10	5.66 ± 0.21
	SON								
NLBright	-9.32 ± 0.08	9.14 ± 0.04	-0.18 ± 0.07	6.70 ± 0.04	-11.27 ± 0.05	-4.57 ± 0.05	16.02 ± 0.08	-20.41 ± 0.07	-4.39 ± 0.09
NLDark	-9.20 ± 0.11	7.01 ± 0.08	-2.20 ± 0.11	6.28 ± 0.06	-10.62 ± 0.04	-4.34 ± 0.07	15.48 ± 0.14	-17.63 ± 0.10	-2.14 ± 0.13
NLDry	-9.01 ± 0.08	11.34 ± 0.03	2.33 ± 0.10	6.61 ± 0.05	-11.09 ± 0.06	-4.47 ± 0.04	15.62 ± 0.11	-22.42 ± 0.04	-6.80 ± 0.11
Aqua	-7.35 ± 0.12	7.29 ± 0.06	-0.07 ± 0.11	7.80 ± 0.11	-7.45 ± 0.03	0.35 ± 0.11	15.15 ± 0.20	-14.74 ± 0.06	0.41 ± 0.20

TABLE S2. Table showing the hemispheric sum of the SFC, TOA, and F_{net} energy in PW for the SH (left), NH (center), and the hemispheric imbalance (NH-SH, right), rounded to the nearest 0.01 PW ($\pm 1\sigma$). Values correspond to integrating under the black (F_{net}), blue (TOA), and green (SFC) curves over each hemisphere in figure 12 of the main text. Positive ΔF_{net} implies energy transport from the NH to the SH.

LIST OF FIGURES

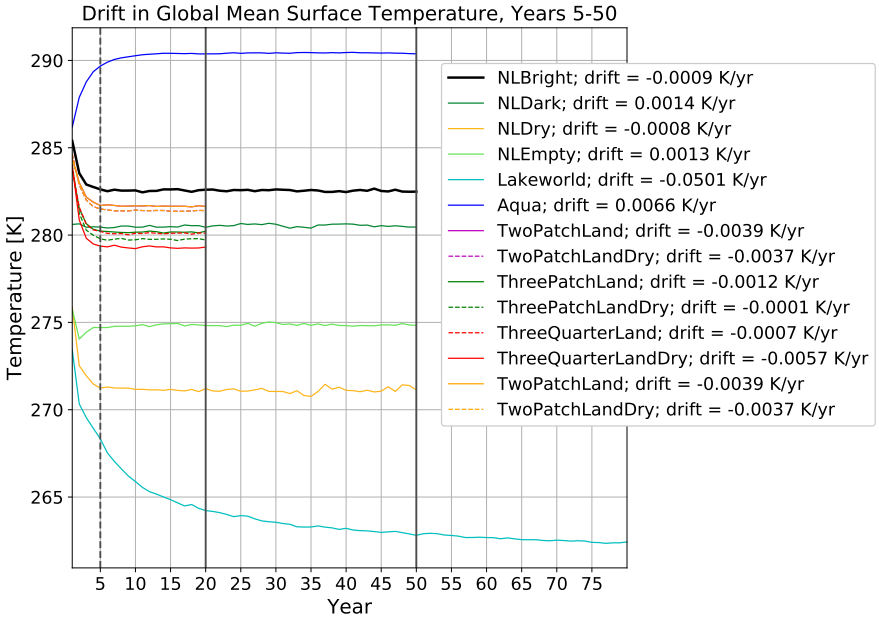

FIG. S1. Spin-up of global mean surface temperatures. The values in the legend show the drift in temperature over the "spun-up" period, are calculated from a linear fit based on years 5 (vertical black dashed line) to 50.

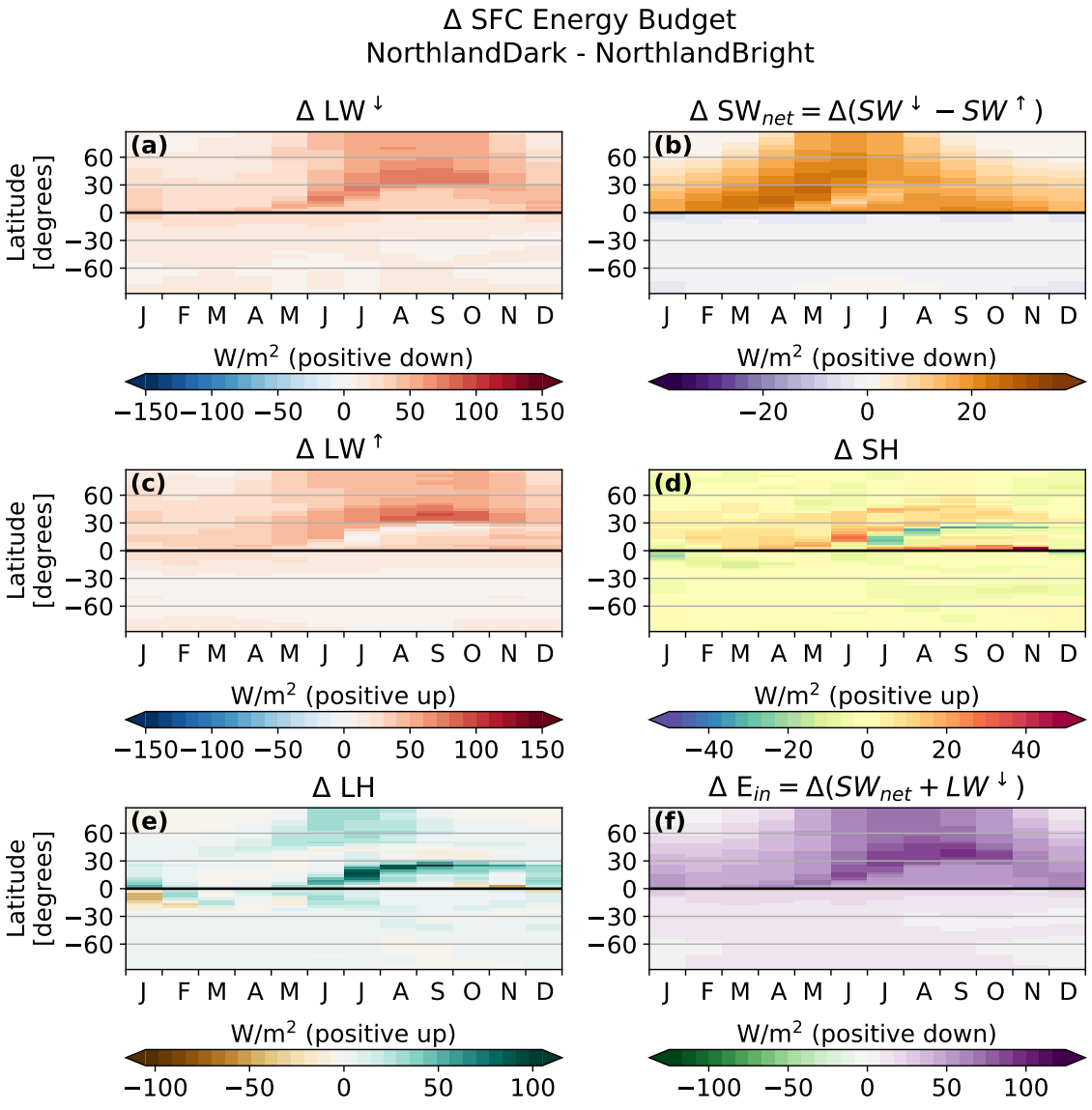

FIG. S2. Change in the zonal mean surface energy budget for NorthlandDark - NorthlandBright over the course of the year. The change in downwards *LW* is shown in (a) while the change in net SFC *SW* is shown in (b). *LW* emitted by the surface is sown in (c), while (d) and (e) show sensible and latent heat, respectively. (f) shows the change in net surface energy uptake ($E_{in} = SW^{\downarrow} - SW^{\uparrow} + LW^{\downarrow}$), where positive values indicate more energy into the surface; in the annual mean this would be balanced by $E_{out} = LW^{\uparrow} + LH + SH$.

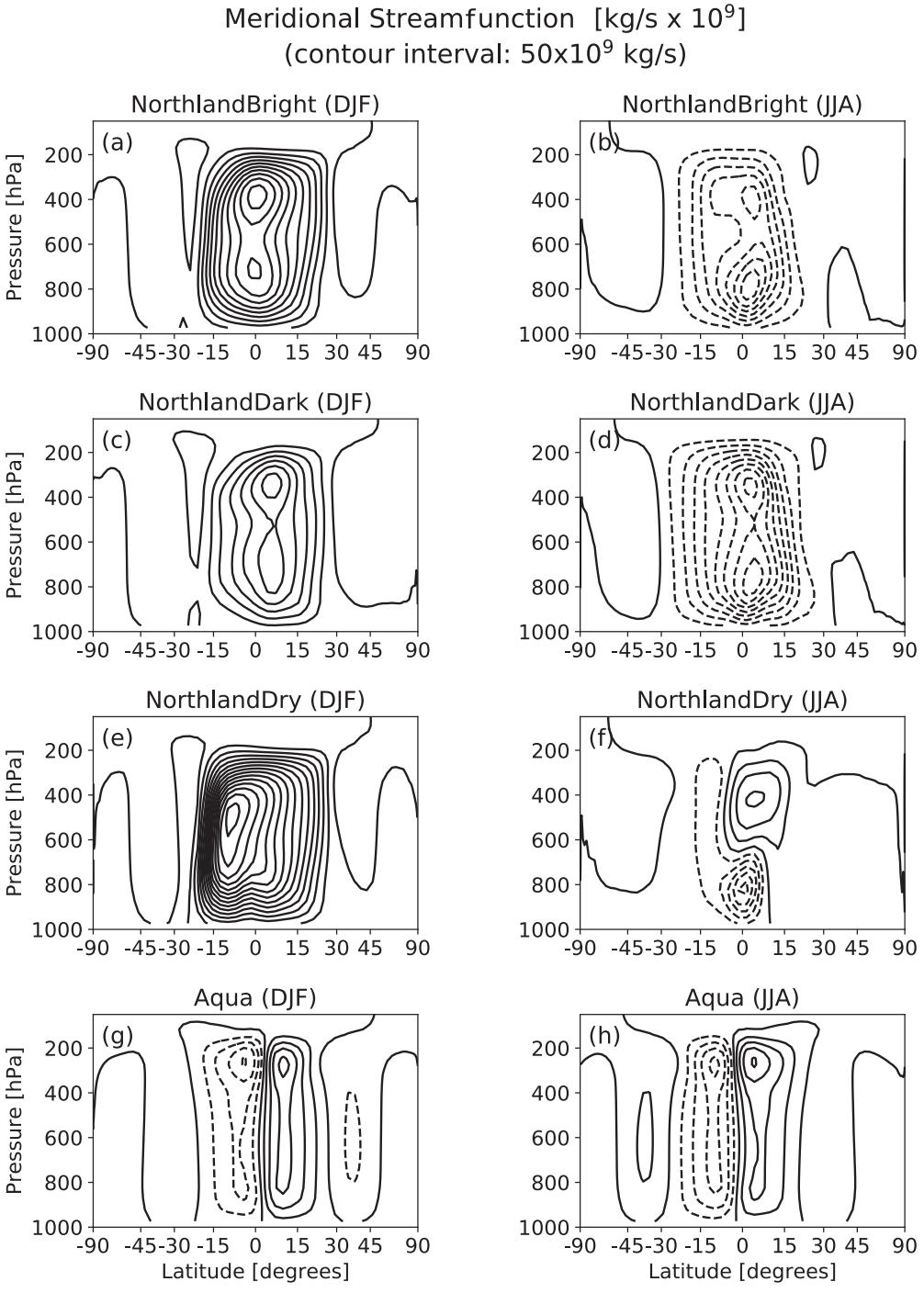

FIG. S3. Meridional streamfunction for DJF (left) and JJA (right) for NorthlandBright (a,b), NorthlandDark (c,d), NorthlandDry (e,f), and Aqua (g,h). Contours are spaced at 50×10^9 kg/s.

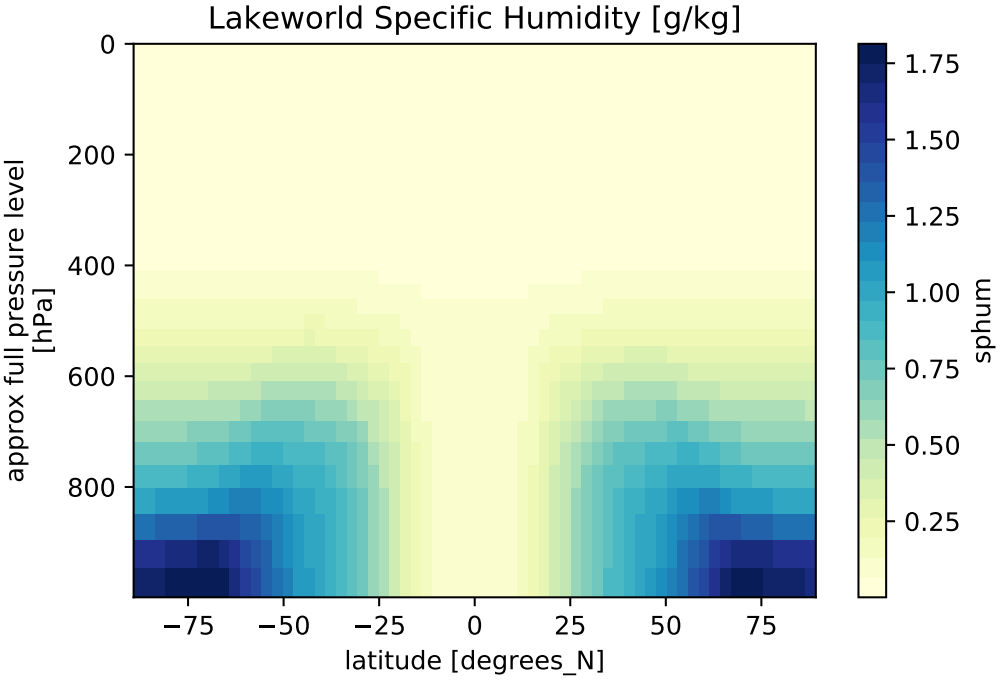

FIG. S4. Cross-section of the zonal mean, annually averaged specific humidity [g/kg] for years 5-50 of the Lakeworld simulation. The atmosphere is very dry except near the surface over the poles, but the peak specific humidity only reaches 1.75g/kg. The specific humidity is near-zero during the polar winter in each heimsphere (not shown). Note that the simulation does not reach equilibrium (see figure S1).

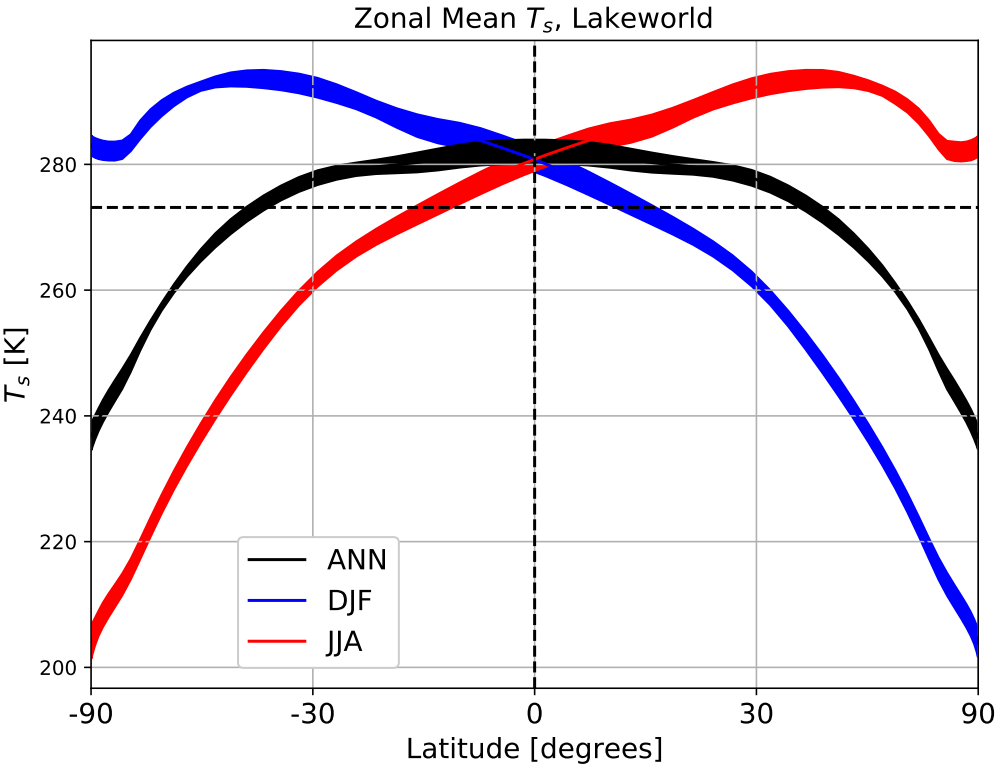

FIG. S5. Zonal mean surface temperature for the Lakeworld simulation. Annual mean temperatures are shown in black, June-July-August temperatures are shown in red, and December-January-February temperatures are shown in blue. Shading shows $\pm 1\sigma$ about the mean of years 5-50. The dashed grey line at 273.15 K shows the freezing temperature of water. Note that Lakeworld is actually cooling over this time period (see figure S1).

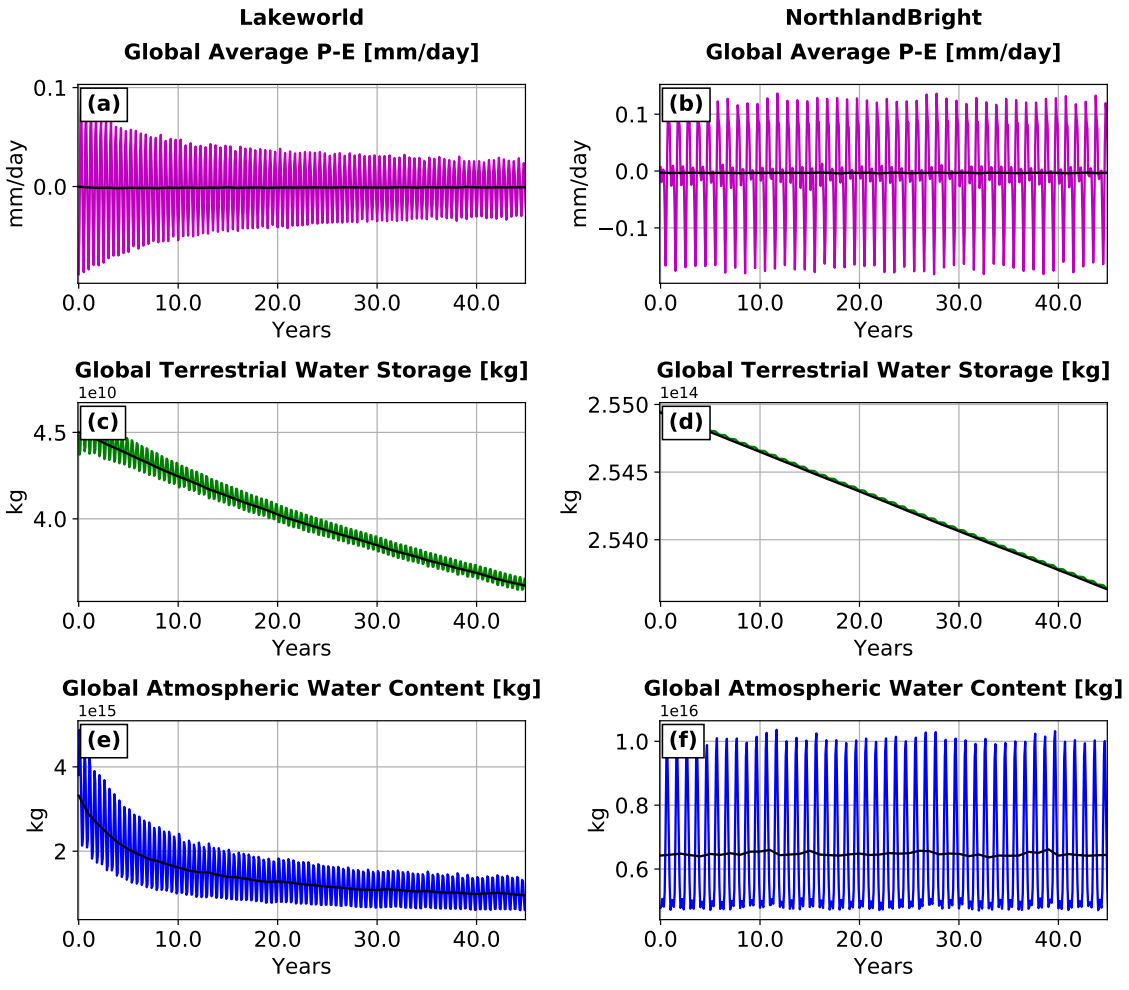

FIG. S6. Figure showing the "leak" of water from the all-land ISCA configuration. Global mean precipitation minus evaporation in mm/day (a,b), integrated terrestrial water storage in kg (c,d), and integrated atmospheric water content in kg (e,f) for Lakeworld (a,c,d) and NorthlandBright (b,d,f). Note the different y-axis ranges for the Lakeworld and NorthlandBright subplots.

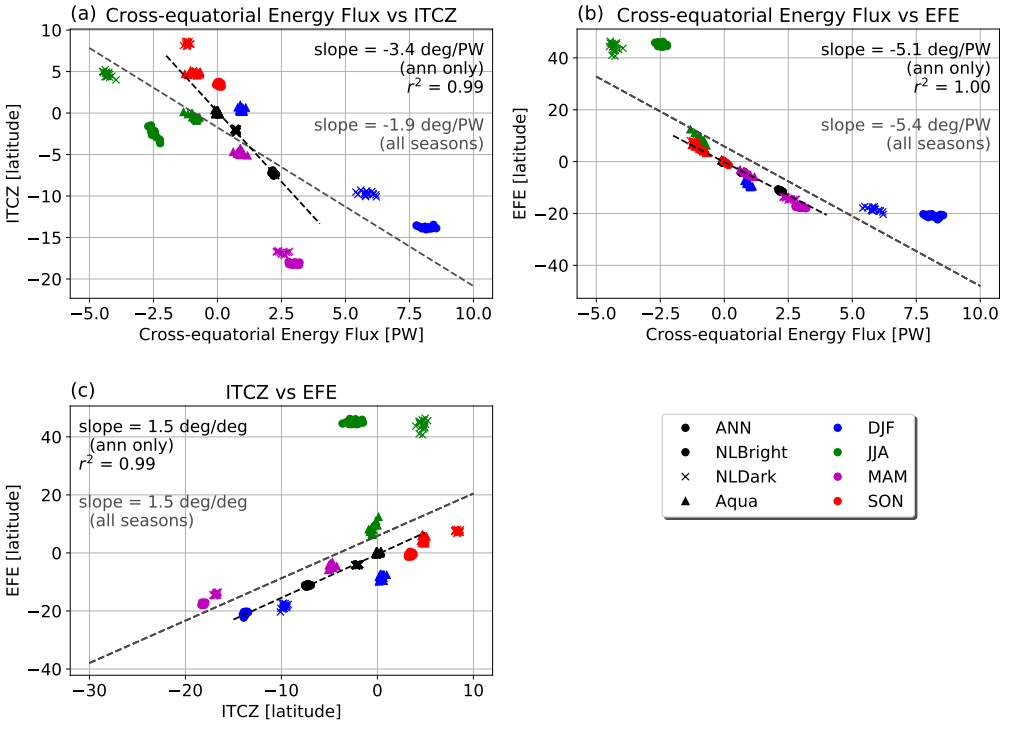

FIG. S7. Relationship between (a) the latitude of the ITCZ and the magnitude of cross-equatorial energy flux, (b) the latitude of the EFE and the magnitude of cross-equatorial energy flux, and (c) the latitude of the EFE and the latitude of the ITCZ. The latitude of the ITCZ is calculated as the center of mass of precipitation between 30°S and 30°N; the latitude of the EFE is calculated as the zonal mean latitude where the vertical integral of polewards atmospheric energy transport $\langle v \cdot h \rangle = 0$; the magnitude of cross-equatorial energy flux is calculated as the magnitude of polewards atmospheric energy transport at the equator ($\langle v \cdot h \rangle_0$). Black markers indicate annual mean values, while blue, purple, green, and red markers indicate DJF, MAM, JJA, and SON averages, respectively. Circles show values for NorthlandBright, x for NorthlandDark, and triangles for Aqua. Each individual marker shows the seasonally averaged value for a single year of the time series. NorthlandDry is not included in the regression calculations here as the ITCZ effectively collapses over the continent.